Czech Technical University in Prague
Faculty of Nuclear Sciences and Physical Engineering
Department of Physics

Diploma Thesis

Miroslav Urbanek

Czech Technical University in Prague
Faculty of Nuclear Sciences and Physical Engineering
Department of Physics

Binary Mixtures in One-Dimensional Optical Lattices

Author: Miroslav Urbanek
Advisor: Ing. Pavel Soldán, Dr.
Year: 2007/2008

Prohlášení

Prohlašuji, že jsem svou diplomovou práci vypracoval samostatně a použil jsem pouze podklady (literaturu, projekty, SW, atd.) uvedené v přiloženém seznamu.

Nemám závažný důvod proti užití tohoto školního díla ve smyslu §60 Zákona č. 121/2000 Sb., o právu autorském, o právech souvisejících s právem autorským a o změně některých zákonů (autorský zákon).

I declare that I have written this diploma thesis independently using the listed references.

V Praze, dne 5. května 2008 ....

podpis

Acknowledgements

I would like to thank my advisor, Ing. Pavel Soldán, Dr. for his valuable advices, great support, and patience during the preparation of this thesis.

Název práce: **Binární směsi v jednodimenzionálních optických mřížkách**

Autor: Miroslav Urbanek
Obor: Matematické inženýrství
Vedoucí práce: Ing. Pavel Soldán, Dr.

Abstrakt: Práca sa zaoberá štúdiom dvojkomponentových zmesí atómov, zachytených v optických mriežkach. Systém je popisovaný binárnym Boseho-Hubbardovým modelom, v ktorom dochádza aj k rôznym fázovým prechodom. Taktiež sú odvodené približné hodnoty jednotlivých parametrov modelu. Systém je analyzovaný pomocou algoritmu “density matrix renormalization group”, ktorý je mimoriadne vhodný pre jednorozmerné systémy. Práca sa zameriava na modelovanie skutočných systémov, ktorých parametre sú dostupné aj experimentálne.

Klíčová slova: Optická mriežka, Boseho-Hubbardov model, binárna zmes, density matrix renormalization group.

Title: **Binary Mixtures in One-Dimensional Optical Lattices**

Author: Miroslav Urbanek

Abstract: A two-component mixtures of atoms, loaded into one-dimensional optical lattices, are studied from theoretical point of view. The binary Bose-Hubbard model is derived from basic principles and its phase transitions are identified. The approximate formulae for model parameters are given as well. The system is analysed using the density matrix renormalization group algorithm, which is a powerful method especially for one-dimensional systems. The work focuses on modelling real systems with experimentally accessible parameter ranges.

Keywords: Optical lattice, Bose-Hubbard model, binary mixture, density matrix renormalization group.

Contents

Preface

The state of matter known as Bose-Einstein condensate was first predicted in the 1920s. It took seventy years to prepare it experimentally. Following the first experimental preparation in 1995, the interest in the field has greatly increased. Many significant advances have been achieved recently. These include progress in laboratory technology - improved cooling, trapping and detection of particles - as well as advances in theoretical description.

One of the results of this scientific endeavour is the invention of *optical lattice*. It utilizes the same principle as an optical trap, which is a device used to confine atoms in small space regions. However, instead of trapping all the atoms at a specific space point, a periodic trapping structure is created. It is possible to create different lattice shapes and even to create low dimensional systems such that atoms are confined to one or two dimensions only.

The system of bosonic atoms confined in an optical lattice can be described by the *Bose-Hubbard model*. Although the model is quite simple, it predicts many properties of a real system. For example, the phase transition between “superfluid” and “insulator” phase predicted by the model [1, 2] has been observed experimentally as well [3].

The current experiments focus on loading atomic mixtures in the optical lattice [4, 5]. Usually, one of the species is a bosonic isotope and the other is either a bosonic or a fermionic isotope. The corresponding two-species Bose-Hubbard model is more complex and exhibits many distinct phase transitions.

Most of the available references deal either with experimental results or with a theoretical analysis of the Bose-Hubbard model with artificial parameters. Only a few of them, for example Ref. [6], focus on theoretical modelling of actual experiments.

This thesis has thus two goals:

- To derive the binary Bose-Hubbard model.
- To analyse the model for a real and feasible experimental configurations, particularly for RbCs and LiCs mixtures in a 1D optical lattice.

The analysis of the Bose-Hubbard model is essentially a many-body problem. The complexity of such problems grows exponentially with increasing particle number. Therefore it is very hard to get any quantitative results even for small systems. However, there exist methods and algorithms that make it possible to obtain results in reasonable time. One of them is the *Density Matrix Renormalization Group (DMRG)* algorithm [7]. This algorithm was used to study the binary Bose-Hubbard model for non-trivial lattice sizes. All the program code was written in the MATLAB$^{®}$ [8] environment by myself.

The topic is intriguing on its own, however, another interesting point is that it encompasses many fields of physics, in particular:

- Atomic physics: fine structure, hyperfine structure
- Quantum optics: interactions of atoms with radiation, optical trap
- Solid state physics: band structure, Wannier functions
- Quantum field theory: many-body Hamiltonian, renormalization
- Scattering theory: interactions between atoms in the lattice
- Statistical physics: density matrix, grand-canonical ensemble
- Computational physics: DMRG

It is clearly not possible to cover all these topics in deserving detail here. Thus only the most important results in connection with optical lattices are compiled in this work. However, the breadth of necessary topics to describe the optical lattice confirms that the nature is not divided into separated fields, but instead forms an integral entity.

Chapter 1

The alkalis

Most experiments with optical lattices are performed using alkali atoms. As we shall show later, the trapping force in an optical trap depends on the properties of transitions between different states of the atom. Alkali transitions lie in the convenient optical part of the spectrum and this makes them experimentally favourable.

Some of their properties can by qualitatively explained in a simplified picture considering atom as a system with a single valence electron moving outside closed electronic subshells. However, detailed analysis of atoms other than hydrogen requires numerical calculation of the wavefunctions, which is a non-trivial task. Precise alkali data are thus acquired from the measurement. This chapter summarizes basic properties of alkalis in connection with optical lattices. Data for different isotopes are given in Table 1.1.

1.1 Bosonic and fermionic isotopes

A neutral atom is a system of Z protons, N neutrons and Z electrons. Protons, neutrons, and electrons are fermions with spin of $1/2$. If the number of all constituent particles is even, the total spin of the atom is integer and the atom is a boson. Likewise, atom with odd number of constituent particles is a fermion. A neutral atom has the same number of protons and electrons, therefore the type of atom depends solely on the number of neutrons - isotopes with even number of neutrons are bosons; isotopes with odd number of neutrons are fermions. Particularly, stable alkali isotopes ^{7}Li, ^{23}Na, ^{39}K, ^{41}K, ^{85}Li, ^{87}Li, and ^{133}Cs are bosons; isotopes ^{6}Li, ^{40}K are fermions.

1.2 Energy spectrum

The energy of an electron in a spherically symmetric Coulombic potential, e.g. in hydrogen atom, depends solely on the principal quantum number n. States with same principal number n, but different orbital angular momentum quantum number l, have identical energy. The situation differs for alkali atoms, where the energy depends also on orbital angular momentum quantum number l.

Transitions in alkali atoms are dominated by transitions of outer electron from it's lowest orbital ns ($l = 0$) to np orbital ($l = 1$). For example, in the case of rubidium, it is a transition from 5s to 5p. This spectral line is called the D line.

Spin-orbit interaction

The spectrum splits into *fine structure* due to the spin-orbit coupling between orbital angular momentum and spin of the valence electron. Fine structure Hamiltonian is

$$H_{FS} = A\mathbf{L} \cdot \mathbf{S} \tag{1.1}$$

where $\mathbf{L}$ is the orbital angular momentum operator, $\mathbf{S}$ is the spin operator, and the value of coupling strength A depends on the electronic configuration. The interaction could be conveniently expressed in terms of total electron angular momentum $\mathbf{J} = \mathbf{L} + \mathbf{S}$. Using an expression

$$\mathbf{J}^2 = \mathbf{L}^2 + \mathbf{S}^2 + 2\mathbf{LS} \tag{1.2}$$

one obtains

$$H_{FS} = \frac{1}{2}A\left(\mathbf{J}^2 - \mathbf{L}^2 - \mathbf{S}^2\right) \tag{1.3}$$

Operator $\mathbf{J}^2$ commutes with $\mathbf{L}^2$ and $\mathbf{S}^2$, and the eigenvalues of the fine structure Hamiltonian could be expressed in a form of quantum numbers as

$$E_{FS}(J, L, S) = \frac{1}{2}A\left[J(J+1) - L(L+1) - S(S+1)\right] \tag{1.4}$$

where J,L and S are total angular, orbital angular and spin quantum numbers, respectively.

According to the angular momentum theory [9], the total angular momentum J can have values in range (electron spin $S = 1/2$):

$$|L - \frac{1}{2}| \leq J \leq L + \frac{1}{2} \tag{1.5}$$

starting from the lowest possible number and spaced by one.

For $L = 0$ there exists just only value of $J = 1/2$ and (1.4) gives $E_{FS} = 0$. Thus the energy level of the s orbital remains unchanged and does not split.

For $L = 1$, one gets two possibilities, $J = 1/2$ and $J = 3/2$. The energy for p orbital splits into two energies with difference:

$$\Delta E_{FS} = \frac{3}{2}A \tag{1.6}$$

The energy levels are usually labeled as $n^{2S+1}\mathrm{X}_J$, where X denotes orbital quantum symbol (S for a state with $L = 0$, P for a state with $L = 1$, etc.). For example, ground state of rubidium is $5^2\mathrm{S}_{1/2}$ and the first two excited states are $5^2\mathrm{P}_{1/2}$ and $5^2\mathrm{P}_{3/2}$.

The D spectrum line in alkali atoms is thus split into a pair D_1 and D_2 corresponding to transitions $n^2\mathrm{S}_{1/2} \rightarrow n^2\mathrm{P}_{1/2}$ and $n^2\mathrm{S}_{1/2} \rightarrow n^2\mathrm{P}_{3/2}$, respectively.

Hyperfine interaction

Another important interaction in alkali atoms is a coupling between the outer-electron angular momentum and the nuclear spin. It gives rise to a *hyperfine structure*. The interaction Hamiltonian, considering only dipole force, is

$$H_{HFS} = B\mathbf{I} \cdot \mathbf{J} \tag{1.7}$$

where $\mathbf{I}$ is the nuclear spin operator, $\mathbf{J}$ is the angular momentum operator, and B is a coupling strength. The coupling strength is not constant and differs for various fine structure orbitals. This Hamiltonian has the same mathematical structure as the spin-orbit interaction Hamiltonian (1.1) and it is thus treated identically.

By introducing total angular momentum operator $\mathbf{F} = \mathbf{I} + \mathbf{J}$, the eigenvalues of the Hamiltonian (1.7) become:

$$E_{HFS}(F, I, J) = \frac{1}{2}B\left[F(F+1) - I(I+1) - J(J+1)\right] \tag{1.8}$$

where F,I and J are the total angular momentum, nuclear spin and angular momentum quantum numbers, respectively. Possible values for F are:

$$|I - J| \leq F \leq I + J \tag{1.9}$$

starting from the lowest possible number and spaced by one.

Nuclear spin I varies for different isotopes and it is determined experimentally. The value of the coupling strength B for different orbitals is obtained from experimental data as well.

For example, rubidium $^{87}\mathrm{Rb}$ has nuclear spin $I = 3/2$. If the atom is in the ground state $5^2\mathrm{S}_{1/2}$, the value of angular momentum is $J = 1/2$. Possible values of total angular momentum are $F = 1$ and $F = 2$. Thus the ground state energy is split into two, with energy difference:

$$\Delta E_{HFS}\left(5^2\mathrm{S}_{1/2}\right) = B\left(5^2\mathrm{S}_{1/2}\right) \tag{1.10}$$

If the atom is in the $5^2\mathrm{P}_{1/2}$ state, the value of angular momentum is $J = 1/2$, too. The level therefore splits into two, with energy difference:

$$\Delta E_{HFS}\left(5^2\mathrm{P}_{1/2}\right) = B\left(5^2\mathrm{P}_{1/2}\right) \tag{1.11}$$

If the atom is in the $5^2\mathrm{P}_{3/2}$ state, F can take values $0, 1, 2, 3$. The state splits into four hyperfine states, and the difference between state with the lowest and with the highest energy is:

$$\Delta E_{HFS}\left(5^2\mathrm{P}_{3/2}\right) = 6B\left(5^2\mathrm{P}_{3/2}\right) \tag{1.12}$$

The $^{87}\mathrm{Rb}$ fine and hyperfine structure scheme is in Figure 1.2.

The difference in energy levels for the hyperfine splitting is very small compared to the fine structure splitting. Moreover, transitions between various states are governed by selection rules. For applications considered here, it is sufficient to restrict possible transitions to the D_1 and D_2 transitions. However, the hyperfine structure plays an important role in atom trapping and collisions.

Figure 1.1: Energy levels diagram for ^{87}Rb.

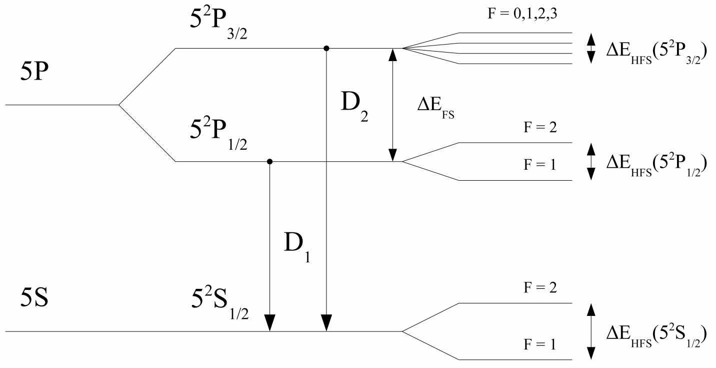

1.3 Hyperfine states

There are many constraints in ultracold alkali atoms experiments. Usually, atoms are cooled down and trapped, but after inelastic collisions some atoms can leave the trap. It is thus important to prepare the experiment in a feasible way.

The trapping, collisional, and many other atom properties depend heavily on its hyperfine state. It was found that only some states have appropriate experimental properties. The atoms are thus prepared in a particular hyperfine state at the beginning of the experiment. The states are usually denoted as $|F, m_F\rangle$, where F is the total angular momentum, and m_F is the projection quantum number. The possible values for m_F are $-F, -F+1, \ldots, F-1, F$.

The most popular states are:

1. $|F = I + 1/2, m_F = F\rangle$ — the double polarized state
2. $|F = I - 1/2, m_F = -F\rangle$ — the maximally stretched state

These hyperfine states have low inelastic scattering rates and can be trapped magnetically [10], thus they are favoured in experiments.

Table 1.1: Alkali isotopes data: name, type (boson or fermion), the proton number Z, the neutron number N, mass m (atomic mass unit u $= 1.661 \times 10^{-27}$ kg), the nuclear spin I, the wavelength of D_2 transition line, the wavelength of D_1 transition line, and the average transition linewidth $\Gamma = \left(\Gamma_{D_1} + \Gamma_{D_2}\right)/2$.

Isotope	Type	Z	N	m [u] [a]	I [b]	D_2 [nm] [c]	D_1 [nm] [c]	Γ [MHz]
^{6}Li	F	3	3	6.01	1	671.0	671.0	36.90 [d]
^{7}Li	B	11	4	7.01	3/2			
^{23}Na	B	19	12	22.99	3/2	589.0	589.6	61.45 [e]
^{39}K	B	19	20	38.96	3/2	766.7	769.9	39.0 [c]
^{40}K	F	19	21	39.96	4			
^{41}K	B	37	22	40.96	3/2			
^{85}Rb	B	37	48	84.91	5/2	780.0	794.8	37.11 [f]
^{87}Rb	B	37	50	86.91	3/2			
^{133}Cs	B	55	78	132.91	7/2	852.1	894.3	30.74 [g]

[a] Ref. [11]
[b] Ref. [10]
[c] Ref. [12]
[d] Ref. [13]
[e] Ref. [14]
[f] Ref. [15]
[g] Ref. [16]

Chapter 2

Optical traps

The confinement of ultracold bosons using optical devices is based on quantum mechanical phenomena. This chapter contains a brief introduction to the optical trap mechanism.

2.1 Optical potential

Optical traps are devices that exploit laser light to trap and confine atoms. They make use of the *AC-Stark effect* - an effect of alternating electric field on energy levels of a neutral atom. In this section a simple semiclassical derivation of formulae describing this phenomenon based on Ref. [10] is presented. The derivation is limited to a linearly polarized light only.

The Hamiltonian of a neutral atom in electric field could be expressed in terms of a multipole expansion. It is assumed that the field is spatially uniform on the atomic scale and thus quadrupole and higher terms can be neglected. The Hamiltonian is then

$$H = H_0 + H' \tag{2.1}$$

where H_0 is the atomic Hamiltonian without the influence of the electric field and H' represents the dipole term of the multipole expansion.

The atom-field interaction H' is given by the correspondence principle as

$$H' = -\boldsymbol{d} \cdot \boldsymbol{\varepsilon}, \tag{2.2}$$

where $\boldsymbol{\varepsilon}$ is the electric field vector, and

$$\boldsymbol{d} = -e \sum_j \boldsymbol{r_j} \tag{2.3}$$

is the electric dipole moment operator for the atomic electrons.

It is assumed that the light propagates in the x direction and that the time-dependent electric-field vector lies in the z direction. Time variation of the electric-field vector, for a fixed point in the x dimension, is $\varepsilon(t) = \varepsilon\left(\mathrm{e}^{i\omega t} + \mathrm{e}^{-i\omega t}\right)$. Therefore the interaction Hamiltonian is

$$H' = -d_z \varepsilon \left(\mathrm{e}^{i\omega t} + \mathrm{e}^{-i\omega t}\right) = -2 d_z \varepsilon \cos \omega t \tag{2.4}$$

The total Hamiltonian H is time-dependent, thus the dynamics of the system could be examined by means of the time-dependent perturbation theory. Suppose that the wave function ψ can be expressed as

$$|\psi(t)\rangle = \sum_n a_n(t) \mathrm{e}^{-iE_n t/\hbar} |n\rangle \tag{2.5}$$

where $|n\rangle$ are eigenkets of H_0, E_n are the corresponding eigenvalues of H_0, and a_n are complex functions of time t. By inserting $|\psi(t)\rangle$ in the Schrödinger equation

$$H|\psi(t)\rangle = i\hbar \frac{\partial}{\partial t} |\psi(t)\rangle \tag{2.6}$$

the set of coupled ordinary differential equations for the coefficients a_n is obtained:

$$i\hbar \dot{a}_n(t) = \sum_k \langle n|H'|k\rangle a_k(t) \mathrm{e}^{i\omega_{nk} t} \tag{2.7}$$

where

$$\omega_{nk} = \frac{E_n - E_k}{\hbar} \tag{2.8}$$

Let us consider an atom initially in a state $|m\rangle$ of the unperturbed Hamiltonian H ($a_m = 1$, and $a_n = 0$ for $n \neq m$), and assume that the electric field is turned on at the time $t = 0$. The equations for coefficients a_n to the first approximation are then

$$a_n^{(1)}(t) = -\frac{1}{i\hbar} \int_0^t dt' \langle n|d_z \varepsilon|m\rangle \left[\mathrm{e}^{i(\omega_{nm}+\omega)t'} + \mathrm{e}^{i(\omega_{nm}-\omega)t'} \right] \tag{2.9}$$

Suppose that the frequency of the electric field is not equal to any of the transition frequencies so the integration can be simply carried out and the expression

$$a_n^{(1)}(t) = -\frac{1}{\hbar} \langle n|d_z \varepsilon|m\rangle \left[\frac{\mathrm{e}^{i(\omega_{nm}+\omega)t} - 1}{\omega_{nm}+\omega} + \frac{\mathrm{e}^{i(\omega_{nm}-\omega)t} - 1}{\omega_{nm}-\omega} \right] \tag{2.10}$$

is obtained.

The expression to the second approximation is found by inserting (2.10) into (2.7). The interesting part is the change of the original state $|m\rangle$. The differential equation for the coefficient $a_m(t)$ is:

$$\begin{aligned} i\hbar \dot{a}_m^{(2)}(t) &= -\frac{2\varepsilon^2}{\hbar} \sum_n \langle m|d_z|n\rangle \langle n|d_z|m\rangle \mathrm{e}^{i\omega_{mn} t} \cos\omega t \left[\frac{\mathrm{e}^{i(\omega_{nm}+\omega)t} - 1}{\omega_{nm}+\omega} + \frac{\mathrm{e}^{i(\omega_{nm}-\omega)t} - 1}{\omega_{nm}-\omega} \right] \\ &= -\frac{2\varepsilon^2}{\hbar} \sum_n |\langle m|d_z|n\rangle|^2 \mathrm{e}^{i\omega_{mn} t} \cos\omega t \left[\frac{\mathrm{e}^{i(\omega_{nm}+\omega)t} - 1}{\omega_{nm}+\omega} + \frac{\mathrm{e}^{i(\omega_{nm}-\omega)t} - 1}{\omega_{nm}-\omega} \right] \end{aligned} \tag{2.11}$$

The coefficient $a_m(t)$ can be also expressed in terms of a complex phase ϕ_m

$$a_m(t) = \mathrm{e}^{-\frac{i}{\hbar}\phi_m(t)} \tag{2.12}$$

Its derivative with respect to time is approximately:

$$\dot{a}_m(t) = -\frac{i}{\hbar}\dot{\phi}_m(t)\mathrm{e}^{-\frac{i}{\hbar}\phi_m(t)} \approx -\frac{i}{\hbar}\dot{\phi}_m(t) \tag{2.13}$$

Hence the derivative of the complex phase in this approximation is:

$$\dot{\phi}_m(t) = i\hbar\dot{a}_m^{(2)}(t) = -\frac{2\varepsilon^2}{\hbar}\sum_n |\langle m|d_z|n\rangle|^2 \mathrm{e}^{i\omega_{mn}t}\cos\omega t\left[\frac{\mathrm{e}^{i(\omega_{nm}+\omega)t}-1}{\omega_{nm}+\omega}+\frac{\mathrm{e}^{i(\omega_{nm}-\omega)t}-1}{\omega_{nm}-\omega}\right] \tag{2.14}$$

The shift in the energy is given by the average rate at which the phase of the state decreases in time. The time average over one oscillation period of the electric field is carried out and the expression

$$\Delta E =< \dot{\phi}_m >_t= -\frac{\varepsilon^2}{\hbar}\sum_n |\langle m|d_z|n\rangle|^2\left[\frac{1}{\omega_{nm}+\omega}+\frac{1}{\omega_{nm}-\omega}\right] \tag{2.15}$$

is obtained.

The energy shift forces the atom to stay at the places of minimal energy. The resulting effect is that the atom is a subject to an *optical potential* $V_0 = \Delta E$. Additionally, it is common to express the electric-field amplitude ε in the terms of the field intensity $I = 2\epsilon_0 c\varepsilon^2$, where ϵ_0 is the vacuum permittivity and c is the speed of light:

$$V_0 = -\frac{I}{2\epsilon_0\hbar c}\sum_n |\langle m|d_z|n\rangle|^2\left[\frac{1}{\omega_{nm}+\omega}+\frac{1}{\omega_{nm}-\omega}\right] \tag{2.16}$$

The simplest analysis of above formula can be given for a two-level atom. If the frequency of the alternating electric field is close to the transition frequency from the ground state $|g\rangle$ to an excited state $|e\rangle$ (ω_{eg}), then the corresponding transition in (2.15) becomes dominant and others can be neglected. Also, the terms with "+" in denominator of (2.15) are much smaller than terms with "−", and can be neglected too (this is called "rotating wave approximation"). It is convenient to introduce the *detuning* $\Delta = \omega - \omega_{eg}$. The positive detuning is called *blue detuning* and the negative one *red detuning*. The expression for the energy shift is then reduced to:

$$V_0 = \frac{I}{2\epsilon_0\hbar c(\omega-\omega_{eg})}|\langle g|d_z|e\rangle|^2 = \frac{I}{2\epsilon_0\hbar c\Delta}|\langle g|d_z|e\rangle|^2 \tag{2.17}$$

The last unknown parameter in the formula above is the dipole matrix element $|\langle g|d_z|e\rangle|$. It can be calculated, if the wavefunctions for $|e\rangle$ and $|g\rangle$ are known. The calculation for alkali atoms is quite complicated because finding exact wavefunctions is a complex problem. However, there is a connection between the dipole matrix element and the natural linewidth of the transition spectral line. Spectral lines are not discrete and in general have a gaussian shape. The natural linewidth is a size of the spectral line at the half maximum. The relation between the natural linewidth Γ and the dipole matrix element is [17]:

$$\Gamma = \frac{\omega_{eg}^3}{3\pi\epsilon_0\hbar c^3}|\langle g|d_z|e\rangle|^2 \tag{2.18}$$

The strength of the optical potential in the two-level-atom approximation is thus:

$$V_0 = \frac{3\pi c^2 \Gamma}{2\omega_{eg}^3} \frac{I}{\Delta} \tag{2.19}$$

The energy shift of atoms in state $|g\rangle$ depends on the detuning of the electric-field frequency Δ and on the field intensity I. The source of alternating electric field in optical traps is usually a laser light. It is simple to focus a laser light on a point in space. Although the light frequency is the same everywhere, the intensity is maximal at the focal point. Therefore the maximal energy shift is also at this point. The blue detuning results in a positive shift, the red detuning in a negative shift. Using a red detuned laser it is therefore possible to trap atoms in the focal point.

Optical potential is, however, quite shallow. Experiments involving optical traps are thus performed with atoms that are precooled to μK range. Because the potential strength is very small, it is often given in units of recoil energy, $E_R = \hbar^2 k^2/(2m)$, where $k = 2\pi/\lambda$ is the light wavevector and m is the particle mass.

Alkali atoms

Obviously, the determination of the optical potential (2.16) for multi-level atoms is more complicated than for a two-level atoms. The polarization of light, selection rules, spectral line intensities, and hyperfine structure play an important role in the calculation. However, there exists a simple approximate formula, if following conditions are met:

1. The detuning is small compared to fine structure splitting, but large compared to the excited state hyperfine splitting.
2. The light is linearly polarized.
3. The saturation is low (cf. next section).

The approximate formula is then [17, 18]

$$V_0 = \frac{\pi c^2 \Gamma}{2\omega_0^3} \left(\frac{1}{\Delta_1} + \frac{2}{\Delta_2} \right) I \tag{2.20}$$

where Δ_1 and Δ_2 are detunings from the D_1 and D_2 lines, respectively, $\omega_0 = \left(\omega_{D_1} + 2\omega_{D_2}\right)/3$ is the weighted average of spectral lines frequency (intensity of D_1 is half of D_2), and $\Gamma = \left(\Gamma_{D_1} + \Gamma_{D_2}\right)/2$ is the average linewidth.

Another important effect is the scattering of trapping light, which leads to the heating of the atomic gas. The scattering rate limits the possible time interval of the optical trap sustainability. The approximate scattering rate is [17]:

$$\gamma = \frac{\pi c^2 \Gamma^2}{2\hbar\omega_0^3} \left(\frac{1}{\Delta_1^2} + \frac{2}{\Delta_2^2} \right) I \tag{2.21}$$

Comparing (2.20) and (2.21) it is clear that the optical potential depends on detuning as $1/\Delta$, whereas the scattering rate as $1/\Delta^2$. It is thus favourable to use a far detuned laser in real experiments, as the gas is less heated and experiments can last longer. Nevertheless, a near detuned laser can be used if the sustainability of the experiment is not an issue. Detailed analysis for binary mixtures of atoms can be found in [18].

2.2 Saturation intensity

An atom interacting with electromagnetic field close to a resonance could absorb a photon and become an excited atom. On the other hand, the spontaneous emission forces an excited atom to emit a photon and deexcite to a lower state. The population of atoms in different states stabilizes when the system reaches equilibrium.

Optical trap is a tool to confine atoms, therefore a change in their state is an undesirable effect. It is thus necessary to estimate the population of different states and to find appropriate trap parameters, so that most of the atoms remain in the ground state.

According to [12], the difference in population densities for a two-level atom is

$$N_1 - N_2 = \frac{N}{1 + I/I_s(\omega)} \tag{2.22}$$

where N_1 is the number of atoms in the first state, N_2 is the number of atoms in the second state, $N = N_1 + N_2$ is the total number of atoms, I is the field intensity, and I_s is the *saturation intensity*. Saturation intensity depends on the frequency of the field ω:

$$I_s(\omega) = \frac{\hbar\omega\omega_0^2}{3\pi c^2} \cdot \frac{(\omega - \omega_0)^2 + \Gamma^2/4}{\Gamma} \tag{2.23}$$

If the field intensity I is small compared to saturation intensity I_s, the population of the first state N_1 is almost equal to the total number of atoms N. Using the above formulas, it is possible to find reasonable intensity of the field that can be used to confine atoms. Alternatively, for a given intensity one obtains suitable detuning frequencies. The saturation intensity has a local minimum in the resonance $\omega = \omega_0$ and increases rapidly if the frequency ω is detuned.

Example

In the seminal experiment with ^{87}Rb atoms [3], authors were able to confine $N = 2 \times 10^5$ atoms in potential depths up to $V_0 = 22E_R$ using laser light with wavelength $\lambda = 852$ nm. The article does not mention power of laser radiation, but the corresponding intensity of the field can by calculated from the given data, and is about $I = 5 \times 10^6$ W m^{-2}. The saturation intensity for given parameters is however much greater, approximately $I_s = 10^{15}$ W m^{-2}. Thus all atoms are safely confined in the ground state.

The next question is how close can the laser be tuned to the resonance, so that a majority of atoms still stays in the ground state. Let k denotes the proportion of atoms in the excited state, $N_2 = kN$. From (2.22) one obtains

$$I_s(\omega) = \left(\frac{1}{2k} - 1\right) I \tag{2.24}$$

and from (2.23) it is possible to calculate the detuning limit for a given k. For the above experimental data and $k = 10^{-6}$, the minimal frequency detuning from D_1 or D_2 line is quite small:

$$\Delta\delta = \lambda - \lambda_0 \approx 3 \text{ nm} \tag{2.25}$$

The parameter magnitudes of this experiment are typical in optical lattices experiments.

The conclusion of this section is that even for a very small laser detunings, the saturation I/I_s is very low. The possible laser wavelengths in optical lattices thus exclude only small regions close to resonances, where the excited states get populated.

Chapter 3

Optical lattices

The optical-trap effect can be used to create a periodic trapping structure — an optical lattice. Instead of focusing the laser light to just one spatial point, where the light intensity has its maximum, the periodic maxima and minima are created. This can be achieved by creating a standing light wave, using a laser and a mirror (Fig. 3.1). The amplitude of electric intensity differs along the x axis and thus a periodic potential for atoms is created. In the case of a red detuned laser, the ground-state energy of atoms is minimal at points of maximal light intensity. The spatial dependency of the electric-field vector in the z direction is

$$\varepsilon(x) = \varepsilon_0 \sin(kx) \tag{3.1}$$

where $k = 2\pi/\lambda$ is the light wave vector. The corresponding field intensity is:

$$I(x) = 2\epsilon_0 c \varepsilon_0^2 \sin^2(kx) = I_0 \sin^2(kx) \tag{3.2}$$

According to (2.20), this gives a lattice potential:

$$V(x) = V_0 \sin^2(kx) \tag{3.3}$$

An optical lattice can be prepared in many ways. The most common approach is to use orthogonally polarized lasers in all three dimensions to create a 3D lattice. However, by using different frequencies and intensities in different directions it is possible to effectively confine atoms in two or one dimensions. It is also possible to create different lattice geometries (rectangular, triangular) by a different laser geometry setup.

Cold atoms interacting with a spatially modulated optical potential resemble in many aspects electrons in an ion lattice potential of a solid crystal. Therefore similar ideas and theory are used in both fields. The main differences are:

- Optical lattices have bigger spacing.
- Optical lattices are mostly defect free.
- They are very easily controlled by laser parameters.

Figure 3.1: Principle of an optical lattice: The standing wave of a laser light creates a periodical trapping potential. The energy shift of the ground state ΔE_g forces bosonic particles to occupy potential wells. The potential depth depends on the laser-light intensity.

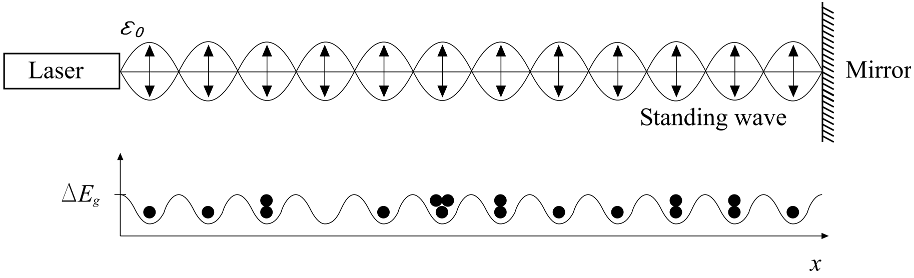

3.1 1D optical lattice

One of the biggest experimental advantages of optical lattices over crystal lattices is the possibility to create lower-dimensional systems. If atoms are confined in transverse dimensions y and z by a strong trap and in x dimension by a weaker optical lattice, the particles are effectively confined in one dimension.

Instead of using strong trap, effective 1D optical lattice is usually realized using optical lattices in all three dimensions. The potential depth in transverse directions is set to higher values than in the x direction. Due to the strong confinement in transverse directions, the tunnelling is possible only in the x direction. The resulting system thus consists of multiple cylindrically shaped 1D systems, as showed in Figure 3.2.

For example, in the experiment [19] the authors were able to create an effective 1D optical lattice by using the optical potential $V_y = V_z = 30E_R$ in transverse directions and the optical potential V_x from $4E_R$ to $14E_R$ in the x direction. The potentials are given in terms of the recoil energy E_R.

One of interesting physical systems that can be engineered in one dimension is a system of impenetrable bosons - Tonks-Girardeau gas [11]. By tuning parameters so that repulsive interactions between atoms get very strong, atoms cannot pass each other and cannot exchange places. The situation resembles cars in a traffic jam. Such bosons have properties similar to fermions but there are important differences in their statistics. Such a system has been realized experimentally [20].

This thesis deals with 1D systems, therefore in the following sections it is assumed that the system is trapped tightly in the directions y and z. The wavefunction is in the ground state in these dimensions. It is thus sufficient to restrict description just to the remaining dimension. However, a few parameters have to be calculated from 3D system description to accurately describe 1D case. These parameters will be pointed out in the appropriate sections.

3.2 Band structure

Optical lattice is a quantum system with a periodic potential. Periodic potentials are extensively studied in the field of the solid state physics, where the most important result is the band structure of the energy spectrum.

Figure 3.2: 1D optical lattice: Optical potential in the y and z directions is much deeper than in the x direction. Atoms are confined in cylindrically shaped regions and hopping between cylinders is suppressed. Every cylinder thus becomes an effective 1D optical lattice.

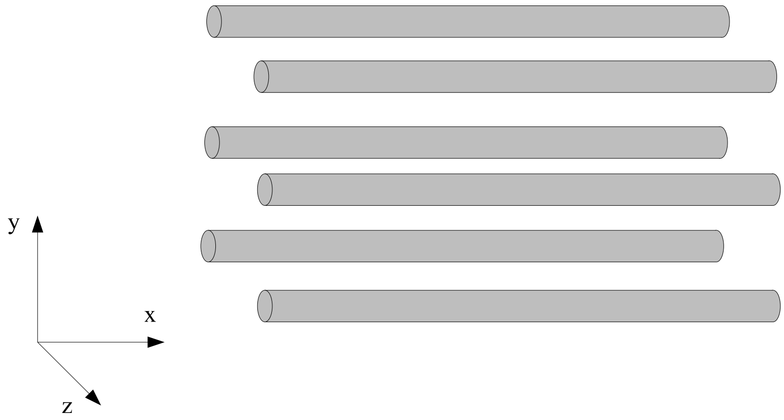

The Hamiltonian of a 1D system with a periodic potential is

$$H = -\frac{\hbar^2}{2m}\nabla^2 + V(x) \tag{3.4}$$

where $V(x)$ is a periodic function with period L. The eigenstates of this Hamiltonian are called Bloch functions

$$\phi_k^{(n)}(x) = e^{ikx}u_{k,n}(x) \tag{3.5}$$

where wave vector k lies in the interval $-\pi/L < k \leq \pi/L$ and functions $u_{k,n}$ are periodic with the period L. The energy bands are numbered by n. Wave vector k defines a particular energy in a band.

The exact properties of the spectrum and eigenfunctions depend on the corresponding potential. The two cases that are usually solved in the solid-state-physics introductory courses are the two limiting cases. In the first one, it is assumed that the potential is very weak and the analysis is carried out perturbatively. This approximation is called *nearly free electron.* The opposing case, called *tight binding*, assumes a very deep potential.

The optical lattice potential is, however, a special one. It has the form

$$V(x) = V_0 \sin^2(kx) \tag{3.6}$$

The characteristic equation for this potential

$$-\frac{\hbar^2}{2m}\nabla\psi(x) + \left[V_0 \sin^2(kx) - E\right]\psi(x) = 0 \tag{3.7}$$

is a differential equation, which arises when dealing with several different problems in physics and which is called *Mathieu equation* [21]. Stable solutions for the Mathieu equation exist just for particular combinations of parameters, in this case V_0 and E. This gives rise to the band structure of energetic spectrum.

Using a program from Ref. [21] for calculating stability regions of Mathieu equation, which is based on the formula from Ref. [22], it is possible to obtain exact energy band diagram (Fig. 3.3). The first few energy bands become very narrow already for moderately deep optical potential.

Figure 3.3: Energy spectrum of an optical lattice depends on optical potential depth V_0. The optical potential and energy are given in terms of the recoil energy. Allowed energy bands are depicted in gray color. A deeper optical potential causes energy bands to become narrower. The dashed red line shows the energy of harmonic oscillator approximation.

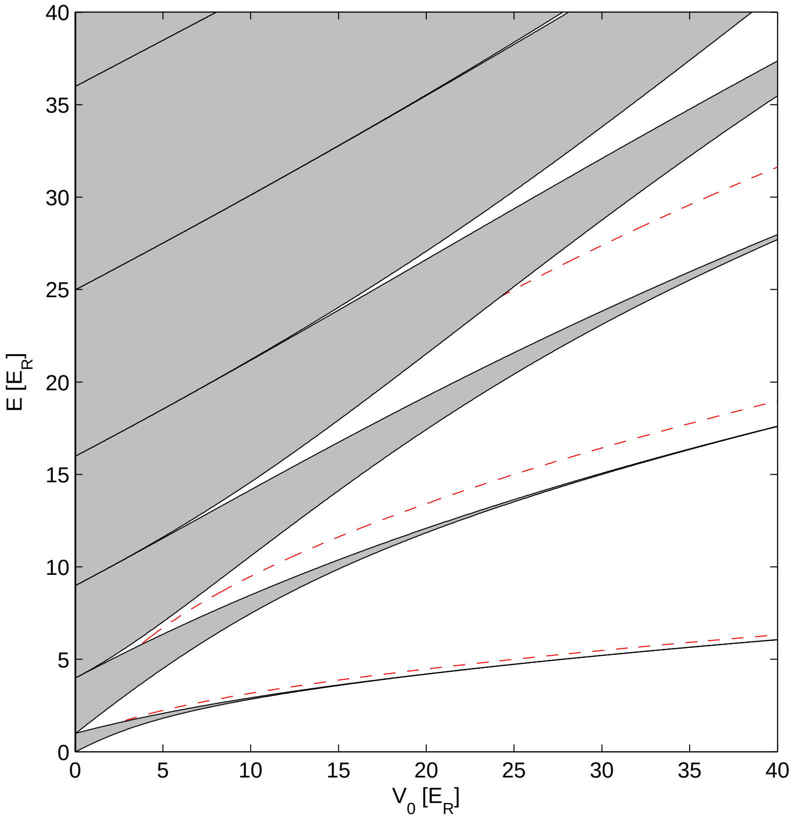

3.3 Wannier functions

Wannier functions [23] are a complete set of real orthonormal functions that can be used instead of Bloch functions to describe a particle in an optical lattice. The descriptions of system using Wannier functions $w_n(x - x_i)$ is equivalent to description using Bloch functions, as there is a transformation between them [23]

$$w_n\left(x - x_i\right) = \sqrt{\frac{L}{2\pi}} \int_{-\pi/L}^{\pi/L} \mathrm{d}k \; \mathrm{e}^{\mathrm{i}kx_i} \phi_k^{(n)}(x) \tag{3.8}$$

where x_i is a position of i^{th} lattice site. The advantage of Wannier functions is the fact they are localized on lattice sites, thus they are more appropriate for description of particles in lattice, especially in deep optical potential.

3.4 Harmonic approximation

Atoms are located around potential minima in deep lattices. At these locations, it is possible to approximate the potential (3.6) with:

$$V(x) \approx V_0 k^2 x^2 \tag{3.9}$$

It is a harmonic potential with frequency:

$$\omega = \frac{2\sqrt{E_R V_0}}{\hbar} \tag{3.10}$$

The energy levels of harmonic approximation can be seen in Figure 3.3 as red dashed lines. Even for moderately deep lattices it is a good approximation of the ground state. Ground state wavefunction in this harmonic approximation is

$$\psi(x) = \left(\frac{1}{\pi a^2}\right)^{1/4} \mathrm{e}^{-\frac{x^2}{2\ell^2}} \tag{3.11}$$

where $\ell = \sqrt{\hbar/(m\omega)}$ is the ground-state size.

Wavefunctions of a harmonic oscillator coincide with Wannier functions (3.8) in this approximation. However, true Wannier functions of potential (3.6) are oscillating at positions distant from lattice center [24]. It must be thus taken into account that the approximation is good around centres of lattice sites but worse elsewhere.

Chapter 4

The Bose-Hubbard model

This chapter introduces a model that describes ultracold interacting particles in an optical lattice. In the first part, interactions between particles are considered. Subsequently, models for one-species gas and two-species gas are derived.

The derivation of models is the same irrespective of the number of dimensions. However, the interaction parameters of the model need to be calculated keeping real physical experiments in mind. Thus the next sections describe a three-dimensional system, and after deriving appropriate model parameters the system is limited to one dimension only.

Lattice experiments are usually performed with atoms in the same hyperfine state. In the next sections it is thus assumed that atoms do not have any internal degrees of freedom. This fact is important for fermions in particular — the atoms are in the same spin state, therefore only single atom can occupy a specific quantum state.

4.1 Interactions between atoms

A distinctive feature of ultracold alkali gases in optical lattices is the particle separation, which is much larger than interparticle interaction range. Under such circumstances, two-body interaction becomes dominant. Moreover, the particles are neutral and thus interact mostly due to van der Waals forces (dipole–dipole forces). Van der Waals interaction potential for distant particles could be approximated by its leading term

$$U(\mathbf{r}) = -\frac{C_6}{|\mathbf{r}|^6} \tag{4.1}$$

where $|\mathbf{r}|$ is the particle distance and coefficient C_6 depends on the interacting species. The effects of interaction can be calculated using scattering theory.

Another assumption that is always met in real experiments is that gas temperature and kinetic energy of particles is very low. It is thus sufficient to limit scattering calculation to the most dominant effect, s-wave scattering. Detailed analysis [10] shows that the interactions could be approximated by pseudopotential

$$U(\mathbf{r}) = g\delta(\mathbf{r}) \tag{4.2}$$

with potential strength

$$g = \frac{2\pi\hbar^2 a}{\mu} \tag{4.3}$$

where a is the scattering length, μ is the reduced mass ($\mu = m/2$ for identical particles with mass m), and δ is the Dirac δ-function.

Strength of a long-range interaction is therefore included in the scattering length a. Accurate values of scattering length, for particular pair of species, are obtained from experimental data. It is important to note that the scattering length could be positive, as well as negative. In the latter case, particles are attracted together and tend to form a region of greater density in the centre of the gas.

Scattering length depends on internal states of interacting atoms. As each alkali atom has a single valence electron, it is common to distinguish two cases — singlet scattering length and triplet scattering length. Singlet and triplet refer to the electronic configurations of interacting atoms. If the atoms are in a particular hyperfine state, the scattering length is a combination of these. Scattering lengths for different isotope pairs are given in Table 4.1.

The data for atomic pairs of same the species have been thoroughly measured for the past ten years. The situation is worse for heteronuclear pairs. Unfortunately, there were no reliable data for RbCs and LiCs atomic pairs at the time of writing. Because binary mixtures are presently a popular research topic, there is a hope that reliable data will be available soon. For example, the data for KRb pairs were measured recently with great accuracy.

The data, given in the Tab. 4.1, are values for free particles. However, scattering length depends on an external potential, and this fact has important experimental consequences. In particular, by using external magnetic field it is possible to tune scattering length. The effect is related to the concept of Feshbach resonances. More details can be found in [10].

4.2 Many-body Hamiltonian

In order to describe a system with a huge number of individual particles contained in an optical lattice, it is necessary to introduce second quantized Hamiltonian. Firstly, let us consider just one particle species with no internal degree of freedom. The field annihilation operator $\Psi(\mathbf{x})$ annihilates a particle at the position $\mathbf{x}$. Annihilation operator and corresponding creation operator $\Psi^\dagger(\mathbf{x})$ have to satisfy commutation relations

$$\begin{aligned} \left[\Psi(\mathbf{x}), \Psi(\mathbf{x}')\right] &= \left[\Psi^\dagger(\mathbf{x}), \Psi^\dagger(\mathbf{x}')\right] = 0 \\ \left[\Psi(\mathbf{x}), \Psi^\dagger(\mathbf{x}')\right] &= \delta\left(\mathbf{x} - \mathbf{x}'\right) \end{aligned} \tag{4.4}$$

in case of bosons and anticommutation relations

$$\begin{aligned} \left\{\Psi(\mathbf{x}), \Psi(\mathbf{x}')\right\} &= \left\{\Psi^\dagger(\mathbf{x}), \Psi^\dagger(\mathbf{x}')\right\} = 0 \\ \left\{\Psi(\mathbf{x}), \Psi^\dagger(\mathbf{x}')\right\} &= \delta\left(\mathbf{x} - \mathbf{x}'\right) \end{aligned} \tag{4.5}$$

in case of fermions.

Table 4.1: Singlet (a_s) and triplet (a_t) scattering lengths for alkali atoms. Bohr radius $a_0 = 5.292 \times 10^{-11}$ m. More confidence is associated with the first value for the RbCs pair.

Isotope pair	a_s $[a_0]$	a_t $[a_0]$	Source
$^{6}\text{Li} \leftrightarrow {}^{6}\text{Li}$	45.5 ± 2.5	-2160 ± 250	[10]
$^{7}\text{Li} \leftrightarrow {}^{7}\text{Li}$	33.2 ± 2	-27.6 ± 0.5	[10]
$^{23}\text{Na} \leftrightarrow {}^{23}\text{Na}$	19.1 ± 2.1	65.3 ± 0.9	[10]
$^{39}\text{K} \leftrightarrow {}^{39}\text{K}$	140^{+3}_{-6}	-17 ± 25	[10]
$^{40}\text{K} \leftrightarrow {}^{40}\text{K}$	105^{+2}_{-3}	194^{+114}_{-35}	[10]
$^{41}\text{K} \leftrightarrow {}^{41}\text{K}$	85 ± 2	65^{+13}_{-8}	[10]
$^{85}\text{Rb} \leftrightarrow {}^{85}\text{Rb}$	2400^{+600}_{-350}	-369 ± 16	[10]
$^{87}\text{Rb} \leftrightarrow {}^{87}\text{Rb}$	90 ± 1	106 ± 4	[10]
$^{133}\text{Cs} \leftrightarrow {}^{133}\text{Cs}$	280 ± 10	2400 ± 100	[10]
$^{39}\text{K} \leftrightarrow {}^{85}\text{Rb}$	33.4	63.9	[25]
$^{39}\text{K} \leftrightarrow {}^{87}\text{Rb}$	1868	35.90	[25]
$^{40}\text{K} \leftrightarrow {}^{85}\text{Rb}$	65.8	-28.55	[25]
$^{40}\text{K} \leftrightarrow {}^{87}\text{Rb}$	-111.5	-215.6	[25]
$^{41}\text{K} \leftrightarrow {}^{85}\text{Rb}$	103.1	349.8	[25]
$^{41}\text{K} \leftrightarrow {}^{87}\text{Rb}$	7.06	164.4	[25]
$^{87}\text{Rb} \leftrightarrow^{133} \text{Cs}$		700^{+700}_{-300} or 176 ± 2	[26]
$^{7}\text{Li} \leftrightarrow^{133} \text{Cs}$	50 ± 20		[27]

Operator $\mathcal{O}_1$, acting on a single-particle wavefunction, can be extended to many particles as in Ref. [28]:

$$O_1 = \int \mathrm{d}^3\mathbf{x}\Psi^\dagger(\mathbf{x})\mathcal{O}_1\Psi(\mathbf{x}) \tag{4.6}$$

Similarly, second quantized form of operator $\mathcal{O}_2$, acting on a two-particle wavefunction is:

$$O_2 = \frac{1}{2}\int \mathrm{d}^3\mathbf{x}_1\mathrm{d}^3\mathbf{x}_2\Psi^\dagger(\mathbf{x}_1)\Psi^\dagger(\mathbf{x}_2)\mathcal{O}_2\Psi(\mathbf{x}_2)\Psi(\mathbf{x}_1) \tag{4.7}$$

4.3 One-species Bose-Hubbard model

The simplest non-trivial model that describes interacting ultracold bosons in a periodic optical potential is the Bose-Hubbard model. It includes the main physics describing strongly interacting bosons, which is governed by the competition between the kinetic and interaction energies. It originates from the Hubbard model, which is very popular in the field of solid state physics, as it describes the transition between the conducting and insulating phases in electron systems. In this section, the model is derived following Ref. [29].

One boson, moving in an optical lattice, is described by the Hamiltonian (3.4). The many-body version is thus:

$$H_J = \int \mathrm{d}^3\mathbf{x}\Psi^\dagger(\mathbf{x})\left[-\frac{\hbar^2}{2m}\nabla^2 + V(\mathbf{x})\right]\Psi(\mathbf{x}) \tag{4.8}$$

Inserting pseudopotential (4.2) into (4.7) gives the interaction Hamiltonian:

$$H_I = \frac{1}{2}\int \mathrm{d}^3\mathbf{x}_1\mathrm{d}^3\mathbf{x}_2\Psi^\dagger(\mathbf{x}_1)\Psi^\dagger(\mathbf{x}_2)U(\mathbf{x}_1-\mathbf{x}_2)\Psi(\mathbf{x}_2)\Psi(\mathbf{x}_1) = \frac{g}{2}\int \mathrm{d}^3\mathbf{x}\Psi^\dagger(\mathbf{x})\Psi^\dagger(\mathbf{x})\Psi(\mathbf{x})\Psi(\mathbf{x}) \tag{4.9}$$

Finally, if the particles are subject to additional external trapping potential $V_T(\mathbf{x})$, trapping contribution to the total Hamiltonian is:

$$H_T = \int \mathrm{d}^3\mathbf{x}\Psi^\dagger(\mathbf{x})V_T(\mathbf{x})\Psi(\mathbf{x}) \tag{4.10}$$

The total Hamiltonian is:

$$H = H_J + H_I + H_T \tag{4.11}$$

The particles are in the ground state, so it is possible to approximate annihilation operator $\Psi(\mathbf{x})$ using the lowest-energy Wannier functions (3.8)

$$\Psi(\mathbf{x}) = \sum_i w_0(\mathbf{x}-\mathbf{x}_i)a_i \tag{4.12}$$

where the annihilation operator a_i annihilates a particle at the lattice site i. Operators a_i satisfy usual bosonic commutation relations:

$$\begin{aligned}\left[a_i, a_j\right] &= \left[a_i^\dagger, a_j^\dagger\right] = 0\\ \left[a_i, a_j^\dagger\right] &= \delta_{ij}\end{aligned} \tag{4.13}$$

Inserting (4.12) into (4.8–4.9), one obtains

$$H_J = -\sum_{i,j} J_{ij} a_i^\dagger a_j \tag{4.14}$$

$$H_I = \frac{1}{2} \sum_{i,j,k,l} U_{ijkl} a_i^\dagger a_j^\dagger b_k b_l \tag{4.15}$$

$$H_T = \sum_i V_i a_i^\dagger a_i \tag{4.16}$$

where tunnelling terms J_{ij}, interaction terms U_{ijkl}, and external trapping terms V_i are given by:

$$J_{ij} = -\int \mathrm{d}^3\mathbf{x}\, w_0(\mathbf{x}-\mathbf{x}_i) \left[-\frac{\hbar^2}{2m}\nabla^2 + V(\mathbf{x}) \right] w_0(\mathbf{x}-\mathbf{x}_j) \tag{4.17}$$

$$U_{ijkl} = g \int \mathrm{d}^3\mathbf{x}\, w_0(\mathbf{x}-\mathbf{x}_i) w_0(\mathbf{x}-\mathbf{x}_j) w_0(\mathbf{x}-\mathbf{x}_k) w_0(\mathbf{x}-\mathbf{x}_l) \tag{4.18}$$

$$V_i = V_T(\mathbf{x}_i) \tag{4.19}$$

The minus sign in J_{ij} is a matter of convention, so that $J_{ij} = J_{ji}$ is positive.

For deep lattice potential the dominant tunnelling terms are $J = J_{ij}\ j = i \pm 1$, describing hopping to a neighbouring site (the on-site hopping terms J_{ii} give just constant shifts in energy levels, thus they are not considered here). The dominant term among interaction terms is the on-site interaction $U = U_{iiii}$. These terms are equal on all lattice sites. Restricting to them gives:

$$H_J = -J \sum_{\langle i,j \rangle} a_i^\dagger a_j \tag{4.20}$$

$$H_I = \frac{U}{2} \sum_i a_i^\dagger a_i^\dagger a_i a_i \tag{4.21}$$

where $\langle i, j \rangle$ denotes neighbouring sites. Using commutation relations (4.13) it is possible to rewrite H_I as:

$$H_I = \frac{U}{2} \sum_i a_i^\dagger \left(a_i a_i^\dagger - 1 \right) a_i = \frac{U}{2} \sum_i n_i \left(n_i - 1 \right) \tag{4.22}$$

where $n_i = a_i^\dagger a_i$ is the particle number operator at the lattice site i.

The total Hamiltonian (4.11) becomes:

$$H = -J \sum_{\langle i,j \rangle} a_i^\dagger a_j + \frac{U}{2} \sum_i n_i \left(n_i - 1 \right) + \sum_i V_i n_i \tag{4.23}$$

A system, described by the Hamiltonian (4.23), is called the Bose-Hubbard model. The difference between a 1D and a 3D lattice is a space arrangement of lattice sites. For a cubic 3D lattice, every site has six nearest neighbouring sites. A 1D lattice is a system of sites arranged in a line, thus there are only two neighbouring sites for every site.

Model parameters

In order to compare theoretical predictions to the experimental results, it is necessary to calculate model parameters U and J (notice that the calculation of V_i from (4.19) is trivial). The right way to do so is to perform a band structure calculation of the optical lattice, find Bloch functions and transform them into Wannier functions. This can be done using solid-state-physics methods.

However, such an approach is not always comfortable. In many situations it is good enough to have an approximate formulae. To calculate on-site interaction energy U it is possible to consider the harmonic approximations of Wannier functions (cf. Section 3.4). The harmonic approximation holds very well for deeper lattices.

Let us assume that there is an optical potential $V_0^{\parallel}$ in the axial direction x and $V_0^{\perp}$ in the transverse directions y and z. The corresponding ground-state sizes of harmonic approximation (3.11) are $\ell^{\parallel}$ and $\ell^{\perp}$, respectively. The ground-state wavefunctions in respective directions are

$$w_x(x) = \left(\frac{1}{\pi {\ell^{\parallel}}^2}\right)^{1/4} \mathrm{e}^{-x^2/\left(2{\ell^{\parallel}}^2\right)} \tag{4.24}$$

$$w_y(y) = \left(\frac{1}{\pi {\ell^{\perp}}^2}\right)^{1/4} \mathrm{e}^{-y^2/\left(2{\ell^{\perp}}^2\right)} \tag{4.25}$$

$$w_z(z) = \left(\frac{1}{\pi {\ell^{\perp}}^2}\right)^{1/4} \mathrm{e}^{-z^2/\left(2{\ell^{\perp}}^2\right)} \tag{4.26}$$

and the corresponding 3D wavefunction:

$$w_0\left(\mathbf{x}\right) = w_x(x) w_y(y) w_z(z) \tag{4.27}$$

Inserting (4.27) into (4.18), one obtains [30]

$$U = U_{0000} = g \int \mathrm{d}^3\mathbf{x}\ w_0^4(\mathbf{x}) = \sqrt{\frac{2}{\pi}} \frac{\hbar^2 a}{m} \frac{1}{{\ell^{\perp}}^2 \ell^{\parallel}} = \sqrt{\frac{2}{\pi^3}} \frac{\lambda a}{{\ell^{\perp}}^2} E_R^{\parallel} \left(\frac{V_0^{\parallel}}{E_R^{\parallel}}\right)^{1/4} \tag{4.28}$$

where λ is the laser wavelength in the axial direction, $E_R^{\parallel}$ is the recoil energy in axial direction and a is the scattering length.

A similar approach could be taken to calculate hopping parameter J [30, 31]. However, true Wannier functions oscillate at places distant from the site origin, which is not the the case of exponential function (4.27). Such an approximation is a source of errors, which can reach an order of magnitude for deep lattices [24]. Fortunately, the hopping term does not depend on transverse confinement and can be calculated from the 1D Mathieu equation assuming a deep potential. The resulting approximate formula is [32]:

$$J = \frac{4}{\sqrt{\pi}} E_R^{\parallel} \left(\frac{V_0^{\parallel}}{E_R^{\parallel}}\right)^{3/4} \mathrm{e}^{-2\sqrt{V_0^{\parallel}/E_R^{\parallel}}} \tag{4.29}$$

Example

Mean-field analysis of the Bose-Hubbard model predicts that a phase transition between the superfluid and Mott insulator phases (cf. next section) occurs at $U/J = 5.8m$, where m is a number of neighbouring lattice sites [1]. In the case of 1D lattice $m = 2$, and thus critical ratio is $U/J = 11.6$. The experimental data from [19] show that a transition begins between optical potential strengths $V_0 = 4E_R$ and $V_0 = 8E_R$ for the chosen experimental setup. Calculation using (4.28–4.29) with parameters from [19], gives a ratio $U/J = 3.9$ for $V_0 = 4E_R$, and $U/J = 14.3$ for $V_0 = 8E_R$. The accordance of the above mentioned prediction and parameter formulae with the experimental evidence is very good.

4.4 Phases of the one-species model

At the zero temperature the physics described by the Bose-Hubbard Hamiltonian can be divided into two different regimes. One is the interaction dominated regime when J is much smaller than U, and the system is in the *Mott insulator* phase. Atoms become localized at the lattice sites. In the $J = 0$ limit, the ground state of the system for a lattice with an integer particle density of ρ atoms per lattice site is described by the wave function [3]

$$|\psi_{MI}\rangle_{J=0} \propto \prod_i \left(a_i^\dagger\right)^\rho |0\rangle \tag{4.30}$$

The other regime is dominated by the kinetic energy — tunnelling overwhelms the repulsion and the system exhibits *superfluid* properties. The particles become delocalized on the whole lattice. The ground state in the $U = 0$ limit, for a lattice filled with M atoms is given by [3]

$$|\psi_{SF}\rangle_{U=0} \propto \left(\sum_i a_i^\dagger\right)^M |0\rangle \tag{4.31}$$

Let us consider the situation, where the system is coupled to the environment and can exchange particles with it. Particle exchange is described using grand-canonical Hamiltonian

$$H' = H - \mu \sum_i n_i \tag{4.32}$$

where H is the Bose-Hubbard Hamiltonian (4.23) and μ is the chemical potential. For high temperatures, it would be necessary to use full statistical density matrix. However, under the assumption that the temperature is very low, the system is with overwhelming probability in the ground state of H'.

The phase diagram (Fig. 4.1) of Bose-Hubbard model in a $J - \mu$ plane includes lobe-like structures [2]. Each Mott lobe is characterized by having a fixed integer particle density ρ. The Mott insulator phases are incompressible, $\partial\rho/\partial\mu = 0$.

Mott insulator phases only occur at integer densities; non-integer density states lie entirely in the superfluid phase because there is always an extra particle that can hop without any energy cost.

Figure 4.1: Schematic phase diagram of the Bose-Hubbard model. It shows two Mott insulator (MI) phases with particle densities $\rho = 1$ and $\rho = 2$, surrounded by the superfluid phase (SF).

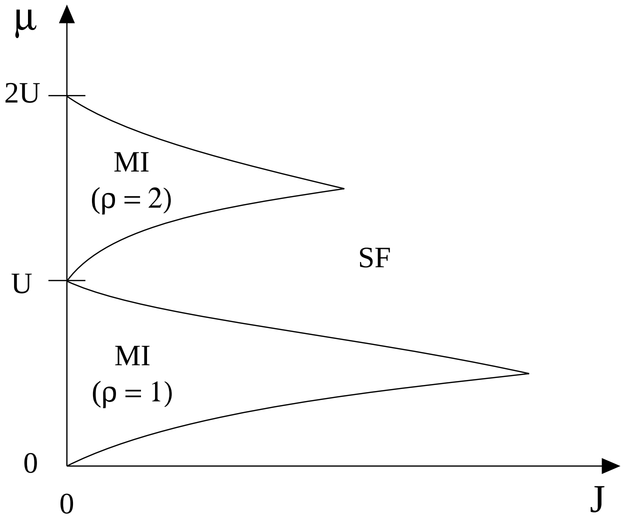

4.5 Two-species Bose-Hubbard model

The optical lattice with two species is more complicated than the one-species case, but the formalism is the same as in the previous section. Let A and B denote particle species, and $\Psi_A(\mathbf{x})$ and $\Psi_B(\mathbf{x})$ respective annihilation operators. Besides commutation relations (4.4–4.5) for each species, they commute mutually [28]:

$$\left[\Psi_A(\mathbf{x}), \Psi_B(\mathbf{x}')\right] = \left[\Psi_A^\dagger(\mathbf{x}), \Psi_B^\dagger(\mathbf{x}')\right] = \left[\Psi_A(\mathbf{x}), \Psi_B^\dagger(\mathbf{x}')\right] = 0 \tag{4.33}$$

Similarly to the previous section, kinetic Hamiltonians for species A and B are:

$$H_{JA} = \int \mathrm{d}^3\mathbf{x} \Psi_A^\dagger(\mathbf{x}) \left[-\frac{\hbar^2}{2m_A}\nabla^2 + V(\mathbf{x})\right] \Psi_A(\mathbf{x}) \tag{4.34}$$

$$H_{JB} = \int \mathrm{d}^3\mathbf{x} \Psi_B^\dagger(\mathbf{x}) \left[-\frac{\hbar^2}{2m_B}\nabla^2 + V(\mathbf{x})\right] \Psi_B(\mathbf{x}) \tag{4.35}$$

Instead of only one interaction Hamiltonian, in this case there are three different interactions between different species ($A \leftrightarrow A$, $B \leftrightarrow B$, and $A \leftrightarrow B$). The interaction Hamiltonians are

$$H_{IAA} = \frac{g_{AA}}{2} \int \mathrm{d}^3\mathbf{x} \Psi_A^\dagger(\mathbf{x}) \Psi_A^\dagger(\mathbf{x}) \Psi_A(\mathbf{x}) \Psi_A(\mathbf{x}) \tag{4.36}$$

$$H_{IBB} = \frac{g_{BB}}{2} \int \mathrm{d}^3\mathbf{x} \Psi_B^\dagger(\mathbf{x}) \Psi_B^\dagger(\mathbf{x}) \Psi_B(\mathbf{x}) \Psi_B(\mathbf{x}) \tag{4.37}$$

$$H_{IAB} = \frac{g_{AB}}{2} \int \mathrm{d}^3\mathbf{x} \Psi_A^\dagger(\mathbf{x}) \Psi_B^\dagger(\mathbf{x}) \Psi_B(\mathbf{x}) \Psi_A(\mathbf{x}) \tag{4.38}$$

where g_{AA}, g_{BB}, and g_{AB} are pseudopotential strengths (4.3).

The external trapping potential is in the same form as before, however, it can differ for different species. If particle A is a subject to a potential $V_{TA}(\mathbf{x})$ and particle B to a potential $V_{TB}(\mathbf{x})$, respective Hamiltonian are:

$$H_{TA} = \int \mathrm{d}^3\mathbf{x}\Psi_A^\dagger(\mathbf{x})V_{TA}(\mathbf{x})\Psi_A(\mathbf{x}) \tag{4.39}$$

$$H_{TB} = \int \mathrm{d}^3\mathbf{x}\Psi_B^\dagger(\mathbf{x})V_{TB}(\mathbf{x})\Psi_B(\mathbf{x}) \tag{4.40}$$

The above terms describe all the effects considered, so the total Hamiltonian for the two species system is:

$$H = H_{JA} + H_{JB} + H_{IAA} + H_{IBB} + H_{IAB} + H_{TA} + H_{TB} \tag{4.41}$$

Approximating annihilation operators with the lowest-energy Wannier functions gives:

$$\Psi_A(\mathbf{x}) = \sum_i w_0^A(\mathbf{x} - \mathbf{x}_i)a_i \tag{4.42}$$

$$\Psi_B(\mathbf{x}) = \sum_i w_0^B(\mathbf{x} - \mathbf{x}_i)b_i \tag{4.43}$$

where annihilation operators a_i and b_i annihilate a particle of species A and B, respectively, in the site i. Besides satisfying commutation relations (4.13) for both species, they satisfy a discrete version of (4.33):

$$\left[a_i, b_j\right] = \left[a_i^\dagger, b_j^\dagger\right] = \left[a_i, b_j^\dagger\right] = 0 \tag{4.44}$$

Using this approximation and restricting to the nearest-neighbour tunnelling in the case of H_{JA} and H_{JB}, and to the on-site interaction in the case of H_{IAA}, H_{IBB} and H_{IAB} gives:

$$H_{JA} = -J_A \sum_{\langle i,j\rangle} a_i^\dagger a_j \tag{4.45}$$

$$H_{JB} = -J_B \sum_{\langle i,j\rangle} b_i^\dagger b_j \tag{4.46}$$

$$H_{IAA} = \frac{U_{AA}}{2} \sum_i a_i^\dagger a_i^\dagger a_i a_i \tag{4.47}$$

$$H_{IBB} = \frac{U_{BB}}{2} \sum_i b_i^\dagger b_i^\dagger b_i b_i \tag{4.48}$$

$$H_{IAB} = \frac{U_{AB}}{2} \sum_i a_i^\dagger b_i^\dagger b_i a_i \tag{4.49}$$

$$H_{TA} = \sum_i V_i^A a_i^\dagger a_i \tag{4.50}$$

$$H_{TB} = \sum_i V_i^B b_i^\dagger b_i \tag{4.51}$$

$$\tag{4.52}$$

Again, $\langle i,j \rangle$ denotes summation over neighbouring sites only. The model parameters are:

$$J_A = -\int \mathrm{d}^3\mathbf{x}\; w_0^A(\mathbf{x}-\mathbf{x}_0)\left[-\frac{\hbar^2}{2m}\nabla^2 + V(\mathbf{x})\right] w_0^A(\mathbf{x}-\mathbf{x}_1) \tag{4.53}$$

$$J_B = -\int \mathrm{d}^3\mathbf{x}\; w_0^B(\mathbf{x}-\mathbf{x}_0)\left[-\frac{\hbar^2}{2m}\nabla^2 + V(\mathbf{x})\right] w_0^B(\mathbf{x}-\mathbf{x}_1) \tag{4.54}$$

$$U_{AA} = g_{AA}\int \mathrm{d}^3\mathbf{x}\;\left[w_0^A(\mathbf{x})\right]^4 \tag{4.55}$$

$$U_{BB} = g_{BB}\int \mathrm{d}^3\mathbf{x}\;\left[w_0^B(\mathbf{x})\right]^4 \tag{4.56}$$

$$U_{AB} = g_{AB}\int \mathrm{d}^3\mathbf{x}\;\left[w_0^A(\mathbf{x})w_0^B(\mathbf{x})\right]^2 \tag{4.57}$$

$$V_i^A = V_{TA}(\mathbf{x}_i) \tag{4.58}$$

$$V_i^B = V_{TB}(\mathbf{x}_i) \tag{4.59}$$

Bosons and fermions

There are two interesting cases for the two-species model:

1. Both species are bosons.
2. One species is a boson (A) and one is a fermion (B).

The difference in the commutation relations between bosons and fermions shows up in the term (4.48), which is zero if B species are fermions. The final form of Hamiltonian is obtained by rearranging terms in (4.47–4.52) and using particle number operators n_i^A and n_i^B for species A and B, respectively, at the site i. In the case of boson-boson mixtures we have the Bose-Bose Hubbard model:

$$\begin{aligned} H = &- J_A\sum_{\langle i,j\rangle} a_i^\dagger a_j - J_B\sum_{\langle i,j\rangle} b_i^\dagger b_j + \\ &+ \frac{U_{AA}}{2}\sum_i n_i^A\left(n_i^A-1\right) + \frac{U_{BB}}{2}\sum_i n_i^B\left(n_i^B-1\right) + \frac{U_{AB}}{2}\sum_i n_i^A n_i^B + \\ &+ \sum_i V_i^A n_i^A + \sum_i V_i^B n_i^B \end{aligned} \tag{4.60}$$

Likewise, for boson-fermion mixtures we have the Bose-Fermi Hubbard model:

$$\begin{aligned} H = &- J_A\sum_{\langle i,j\rangle} a_i^\dagger a_j - J_B\sum_{\langle i,j\rangle} b_i^\dagger b_j + \frac{U_{AA}}{2}\sum_i n_i^A\left(n_i^A-1\right) + \frac{U_{AB}}{2}\sum_i n_i^A n_i^B + \\ &+ \sum_i V_i^A n_i^A + \sum_i V_i^B n_i^B \end{aligned} \tag{4.61}$$

Model parameters

The formulae for the hopping parameters J_A and J_B, as well as formulae for homonuclear on-site interaction U_{AA} and U_{BB} are the same as in the one-species model. It is thus possible to use (4.28–4.29) with constants for the A and B species to calculate J_A,U_{AA} and J_B,U_{BB}, respectively.

To calculate heteronuclear on-site interaction U_{AB}, a similar approach as in the one-species case is taken. The Wannier functions are approximated by harmonic-oscillator eigenfunctions (4.24–4.27). The functions are different for different species. Inserting them into (4.57) and carrying out the integration gives:

$$U_{AB} = \frac{2\hbar^2 a}{\sqrt{\pi}} \frac{m_A + m_B}{m_A m_B} \frac{1}{\left({\ell_A^\perp}^2 + {\ell_B^\perp}^2\right)\sqrt{{\ell_A^\parallel}^2 + {\ell_B^\parallel}^2}} \tag{4.62}$$

where a is the interspecies scattering length, $m_{A,B}$ are species masses, and $\ell_{A,B}^{\perp,\parallel}$ are the ground site sizes in transverse and axial directions. Of course, U_{AB} depends on the strength of the optical potential, because the ℓ terms depend on it as well.

4.6 Phases of the two-species model

The number of distinct phases in the two-species model is much bigger than in the one-species case. Besides the Mott insulator and the superfluid phase for each of the species, some additional phases were identified in the two-component mixtures [33, 34]:

1. **Charge density wave**: Atoms are localized on lattice sites and the species are alternating (A,B,A,B,. . .).
2. **Phase separation**: Atoms are localized on lattice sites and the same species stick together (A,A,. . . ,B,B).
3. **Supersolid**: Atoms are delocalized and species are alternating (A,B,A,B,. . .).

Finding a phase diagram for arbitrary parameters is a complex task, because the two-species Bose-Hubbard model has many free parameters. However, it is possible to get an insight into the important effects by studying the limiting cases.

Deep lattice limit

One of the important special cases is the case of a very deep lattice. The role of hopping between sites is diminished in this case. It is thus interesting to analyse two-species Bose-Hubbard model for vanishing hopping terms $J_A = J_B = 0$. Because hopping is not possible, the atoms cannot move to the neighbouring sites. It is sufficient to analyse one site only and neglect external trapping potential, $V_A = V_B = 0$. The Bose-Bose Hubbard Hamiltonian (4.60) in this limit is:

$$H = \frac{U_{AA}}{2} n^A \left(n^A - 1\right) + \frac{U_{BB}}{2} n^B \left(n^B - 1\right) + \frac{U_{AB}}{2} n^A n^B \tag{4.63}$$

Let us consider the system is coupled to the environment and can exchange particles with it. Particle exchange is described using grand-canonical Hamiltonian

$$H' = H - \mu_A n^A - \mu_B n^B \tag{4.64}$$

where μ_A and μ_B is the chemical potential for species A and B respectively. Varying the chemical potentials μ_A and μ_B, the ground state number of particles varies as well. The phase diagrams for various combination of parameters U_{AA},U_{BB}, and U_{AB} can be seen in Figures 4.2 and 4.3.

The deep lattice limit gives an important insight into the phase diagram even for moderate lattices. In real lattices the transition between different particle numbers is gradual, thus there are intermediate transition regions between regions with constant particle numbers.

Figure 4.2: Phase diagrams in deep lattice limit: μ_A and μ_B are chemical potentials for species A and B. The separated regions correspond to different particle numbers of both species. Along the μ_A axis, the particle number of species A varies from 1 to 3. Similarly, the particle number of species B varies along the μ_B axis from 1 to 3. The regions in the centre of the figures correspond to states occupied by both species.

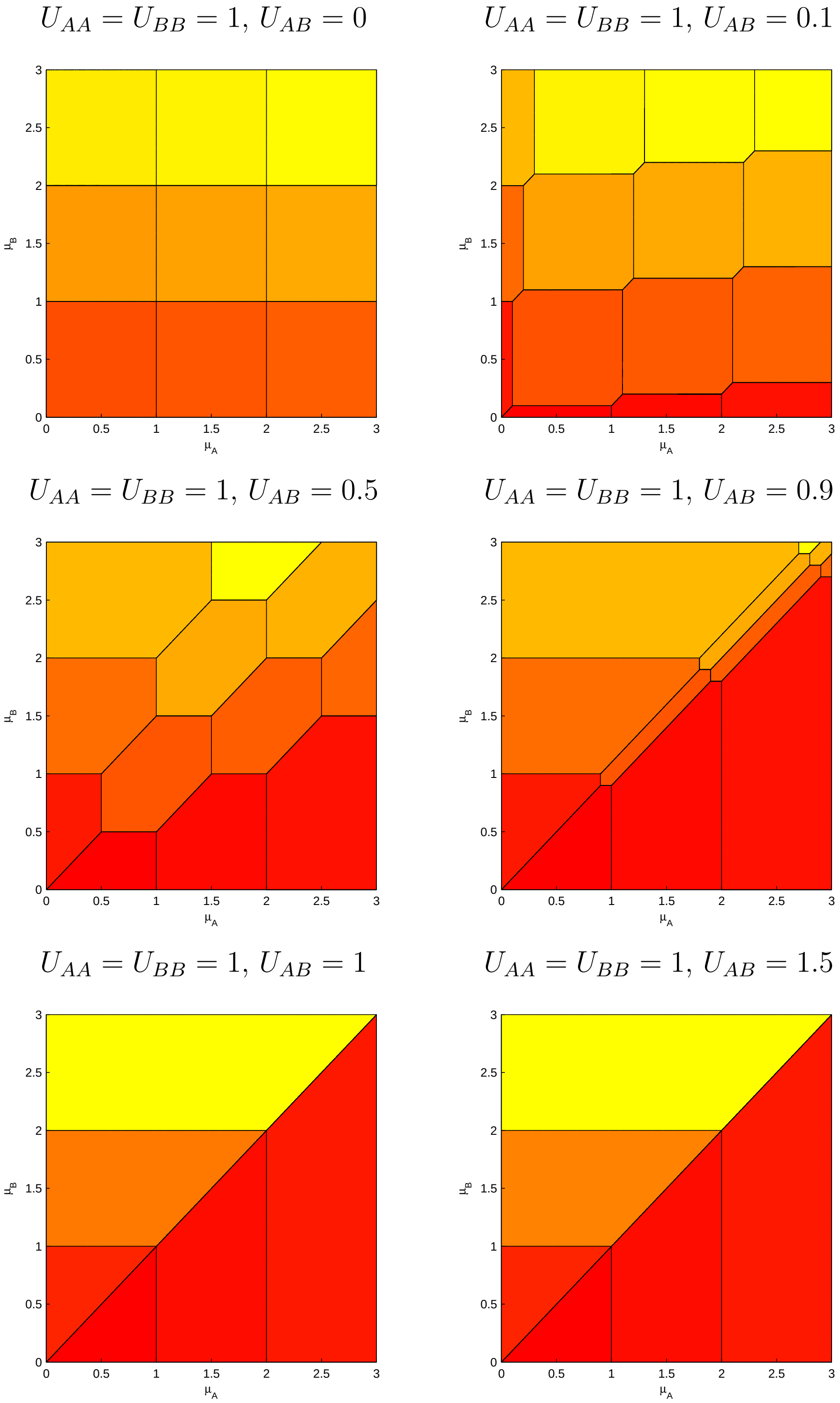

$U_{AA} = U_{BB} = 1,\ U_{AB} = 0$

$U_{AA} = U_{BB} = 1,\ U_{AB} = 0.1$

$U_{AA} = U_{BB} = 1,\ U_{AB} = 0.5$

$U_{AA} = U_{BB} = 1,\ U_{AB} = 0.9$

$U_{AA} = U_{BB} = 1,\ U_{AB} = 1$

$U_{AA} = U_{BB} = 1,\ U_{AB} = 1.5$

Figure 4.3: Phase diagrams in deep lattice limit: μ_A and μ_B are chemical potentials for species A and B. The separated regions correspond to different particle numbers of both species. Along the μ_A axis, the particle number of species A varies from 1 to 3. Similarly, the particle number of species B varies along the μ_B axis from 1 to 2. The regions in the centre of the figures correspond to states occupied by both species.

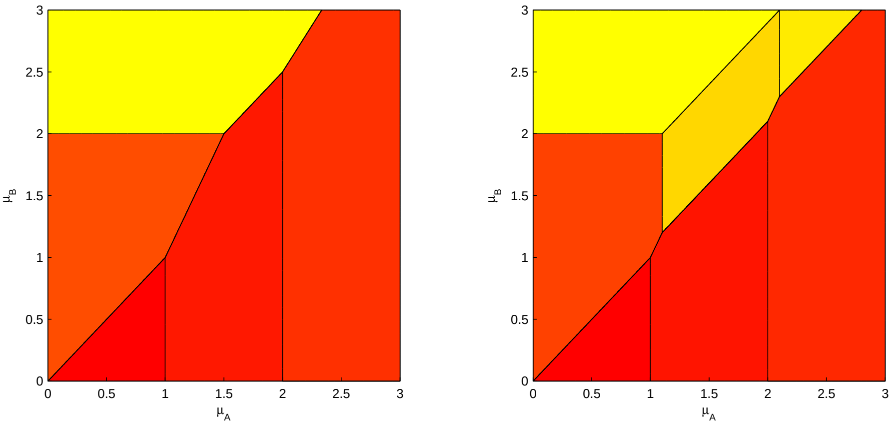

$U_{AA} = 1$, $U_{BB} = 2$, $U_{AB} = 3$

$U_{AA} = 1$, $U_{BB} = 2$, $U_{AB} = 1.1$

Chapter 5

Density matrix renormalization group algorithm

The problem of finding bound states of a quantum system is one of the most fundamental problems in the field of quantum physics. The basic approach is to construct the Hamiltonian and to diagonalize it. In special cases this can be done analytically. However, only a small number of interesting Hamiltonians can be solved this way. A perturbative approach is also useful in certain cases, but only if the perturbations are very small. The only method, which is applicable almost in all cases is a numerical approach — for example, to construct the matrix Hamiltonian and to find its eigenstates. There are two important issues:

1. As many systems have infinite number of allowed states, the number of base vectors has to be truncated to a finite number. Only the most essential states have to be retained. A question is *what are the most important states*. The answer depends on the bound states one is interested in. If the problem is to find the ground state, that is the state with minimal energy, the most important base vectors to retain are the vectors of minimal energy.

   For example, in the case of the Bose-Hubbard model (4.23), the number of particles on one site can be infinite. Nevertheless, it is clear that if the interaction term U is positive, the states with more particles on the site have higher energy. Thus if one wants to find the ground state of this model, it is reasonable to limit the number of allowed particles on the site.

2. If the quantum system is composed of subsystems, the total Hilbert space is the tensor product of Hilbert spaces of the subsystems. The total space dimension is a product of the corresponding subsystem dimensions. As the number of subsystems increases linearly, the dimension of total space increases exponentially. Thus, for a big system, it is very complicated to diagonalize the matrix Hamiltonian, because of the matrix size. This is called the *many-body problem*.

   For example, consider the Bose-Hubbard model and limit the number of particles on the site to $n = 5$. If the system has N sites, the dimension of the total space is $d = n^N$. For the system of $N = 10$ sites this gives dimension $d = 9765625$. Obviously, it is very complicated to create, store and diagonalize such a big matrix. Even small system of $N = 10$ sites and $n = 5$ maximum particles per site is in fact too complex for numerical computation on most of today's computers.

In the case of ultracold physics, one is usually interested in the ground state properties. Thus the solution to the first issue is clear - limit the number of particles on-site.

There are many approximate methods how to overcome the second issue, the many-body problem, for example *mean field theory* model or *quantum Monte Carlo*. However, there exists an approach which is powerful especially for one-dimensional problems - the *Renormalization Group* approach. The focus of this thesis is primarily on this approach and on a particular method called the *Density Matrix Renormalization Group (DMRG)* algorithm [35, 36, 7].

The basic idea of renormalization group methods is quite simple - to divide the system into blocks and to treat every block separately, considering interactions between blocks. Only a fixed number of states is retained in every block. The way of creating the blocks and choosing the retained states characterizes the particular renormalization group method.

5.1 Blocks renormalization group algorithm

The basic method is a *Blocks Renormalization Group (BRG)* algorithm in one dimension. Consider a lattice system and let m be the number of states kept in a block. Then the BRG algorithm is [7]:

1. Describe interactions on an initial sublattice ("block") A of length l by a block Hamiltonian H_A acting on an m-dimensional Hilbert space.
2. Form a compound block AA of length $2l$ and the Hamiltonian H_{AA}, consisting of two block Hamiltonians and interblock interactions. H_{AA} has dimension m^2.
3. Diagonalize H_{AA} to find the m lowest-lying eigenstates.
4. Project H_{AA} onto the truncated space spanned by the m lowest-lying eigenstates, $H_{AA} \to H'_{AA}$.
5. Restart from step (2), with doubled block size: $2l \to l$, $AA \to A$, and $H'_{AA} \to H_A$, until the lattice size is reached.

The most time consuming part of this algorithm is the diagonalization of H_{AA}. In every block only m lowest-lying states are retained, and thus the size of matrix Hamiltonians H_{AA} is always the same. The complexity of the algorithm grows linearly with doubling the block length. Without the truncation of high-energy states the system would grow exponentially, thus the improvement is significant.

However, the outlined procedure gives very poor results for certain problems. The breakdown can best be understood visually (Fig. 5.1): assuming an already rather large block size, where discretization can be neglected, the lowest-lying states of the left block all vanish at the compound block center. The true ground state

Figure 5.1: Poor results of the BRG: All the states lying in the left and right block have boundary conditions such that the wavefunction vanishes at the block boundary. These states cannot accurately represent low lying states of the compound block.

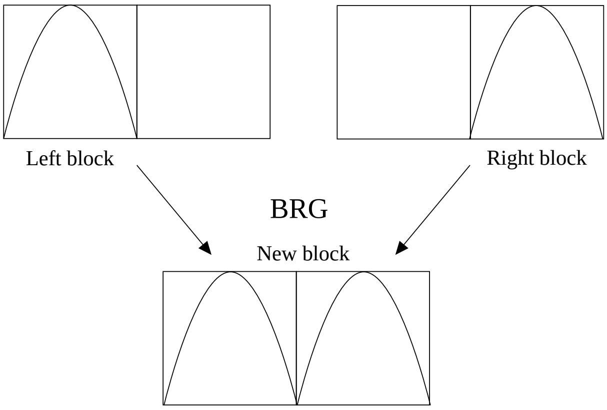

of a new block has its maximum amplitude right there, thus it cannot be properly approximated by a combination of the states from the left and right blocks only.

The problem lies in the inappropriate boundary conditions imposed on the states in both blocks. The blocks cannot be treated as independent systems. They have to be embedded in some environment.

5.2 Density matrix renormalization group algorithm

The boundary condition problem could be solved by introducing an interaction between the block and the environment. Instead of finding the ground state of the block alone, the compound system of the block and the environment is constructed — the *superblock*. The ground state of the superblock is found, projected onto the block and then the block space is truncated. The question is how to perform the projection and the truncation.

The compound system space is a tensor product of the block space and the environment space. A pure state in the compound space is expressed as

$$|\psi\rangle = \sum_{i,j} \psi_{i,j} |\alpha_i\rangle \otimes |\beta_j\rangle \tag{5.1}$$

where $|\alpha_i\rangle$ for $i = 1, \ldots, m$ and $|\beta_j\rangle$ for $j = 1, \ldots, n$ are base vectors of the block space and the environment space, respectively. The state is generally an entangled state for the block and the environment, therefore it could not be simply described as a single block state or a single environment state. Nevertheless, the block states, which best describe the ground state of the superblock, are sought.

The key is to trace environment out and to construct reduced density matrix ρ_B

for the block [7]:

$$\langle \alpha_{i'} | \rho_B | \alpha_i \rangle = \sum_j \psi^*_{i,j} \psi_{i',j} \tag{5.2}$$

ρ_B essentially describes the states on the block, which belong to the ground state on the superblock. The density matrix is positive-semidefinite, self-adjoint and has a unit trace. ρ_B has m eigenvalues $w_i \geq 0$ and respective eigenstates $|\gamma_i\rangle$, with $\sum_i w_i = 1$.

The most relevant states are the states with the highest eigenvalues of the density matrix. Therefore in the truncation of the block space it is most reasonable to retain these states as they best describe the ground state of the superblock in the block space.

1D system

The DMRG for 1D system is briefly outlined here. The BRG algorithm, described in Section 5.1, uses exponential growth of the system. For the DMRG algorithm the linear growth is more appropriate, that means instead of doubling the block every step it is better to add one site at the time. 1D system is a chain with interactions between sites:

$$\bullet - \bullet - \bullet - \bullet.$$

Adding one site at the time, the block becomes:

$$\bullet - \bullet - \bullet - \bullet - \circ.$$

There are many ways how to select and describe environment. A good approach in 1D case is to use the same type of system, inverted [36]:

$$\bullet - \bullet - \bullet - \bullet - \circ - \circ - \bullet - \bullet - \bullet - \bullet.$$

The right and left part could be represented as blocks:

$$L - \circ - \circ - R.$$

Let m be the number of states kept in a block and n be the number of allowed states on a site. One DMRG step works as follows [7]:

1. Describe interactions on the left block L and on the right block R by a block Hamiltonians H_L and H_R acting on an m-dimensional Hilbert spaces.

2. Describe interactions on the left and right central sites by Hamiltonians H_{CL} and H_{CR}.

3. Form a compound superblock and respective Hamiltonian H_{SB}, consisting of the left block, left central site, right central site and right block Hamiltonians and interactions between them. H_{SB} has dimension $m^2 n^2$.

4. Diagonalize H_{SB} to find its ground state.

5. Create the density matrix for the left part (left block and central left site combined).

6. Find m density-matrix eigenstates with the highest eigenvalues.
7. Project the left part Hamiltonian (combination of H_L and H_{CL}) onto the m-dimensional truncated space spanned by these eigenstates.
8. Do the steps 5-7 for the right part as well.

If the size of the original block (number of included sites) was l, the new block size is $l + 1$.

There are several methods for calculating parameters of physical systems using this algorithm. One approach, *infinite-system DMRG*, is used for very long chains. The size of the block is increased in every step. The other approach, *finite-system DMRG*, is used for finite-length systems. We will deal with the latter case only.

Warmup

The first step in finite-system DMRG is a warmup phase - preparing block data (Hamiltonians and operators describing interactions with adjacent site) for different system lengths. Repeating the above process from an initial small block, the size of the system grows at the rate of two sites in a step (left and right block grows by one site each). The block data for different system sizes are stored. The process is repeated until the size of the left and right blocks and the two sites between them reaches the size of the system N:

$$L(N/2-1) - \circ - \circ - R(N/2-1),$$

where $L(n)$, $R(n)$ are the left and right blocks containing n sites.

Sweep

During a sweep, the division point between the left and right parts moves in both directions. Firstly to the right; new left blocks are created:

$$L(n) - \circ - \circ - R(N-n-2) \to L(n+1) - \circ - \circ - R(N-n-1),$$

When the smallest possible right block is reached, the sense of motion is inversed and the right blocks for various partitioning of the system are created or updated:

$$L(n) - \circ - \circ - R(N-n-2) \to L(n-1) - \circ - \circ - R(N-n-3),$$

When the smallest possible left block is reached, the sense is inverted one more time. The left blocks are updated until the division point reaches the center of system.

In one sweep, the block data for all possible divisions of the chain are updated. The sweeping process is repeated a few times. The block data and values of various observables usually converge after several steps.

Boundary conditions

Important parts of the model are the boundary conditions imposed at the ends of the lattice. There are two basic types of boundary conditions for a 1D lattice:

1. Open boundary condition: the site at the end of the lattice interacts only with the site in the direction to the centre of the lattice.
2. Periodic boundary condition: the site at the end of the lattice interacts artificially with the site at the other end of the lattice.

To simulate a long lattice, a periodic boundary condition would be a better choice. However, it was found out that the calculation using a periodic boundary condition is far less accurate [7]; there could be a difference of several orders of magnitude. Moreover, the Bose-Hubbard model (4.23) with external trapping potential ($V_i \neq 0$) is not translationally invariant, therefore a periodic boundary condition is not appropriate in this case.

For these reasons, the open boundary condition was always used in the actual DMRG implementation.

Convergence

The DMRG algorithm is clearly not an exact algorithm. There is no mathematical proof that the calculation will converge to the correct ground state. However, trial calculations show that the method usually performs very good.

For example, Ref. [37] compares the exact solutions of the Hubbard model using Bethe ansazt to the results of the DMRG calculation. The authors found out that the relative error is below 0.3% for their calculation parameters. Another integrable model, a single particle in a harmonic potential, was analyzed in Ref. [38], and again the exact solution and DMRG calculation yielded very similar results.

However, most of the interesting models are not exactly solvable. The authors usually compare the exact diagonalization results of a system of few (5–40) lattice sites with a DMRG calculation on the same system. The results of the calculation are very accurate and this fact gives them confidence, that the calculation is precise for longer lattices as well [35].

Although the trust in the method is quite strong, a DMRG practitioner must keep in mind that the method is not a “black box” that gives good results with high precisions in every case. All the results have to be scrutinized for possible errors.

5.3 Implementation details

The detailed description of the DMRG algorithm can be found in Ref. [36, 38, 7, 39]. This section discusses important points of the actual implementation.

Site Hamiltonian

The Bose-Hubbard model describes a chain of lattice sites. If the particles in the model are bosons, the number of particles located on any site is unlimited. However, for practical purposes it is necessary to limit this number — let M be the maximum number of particles located on a single lattice site (M_A and M_B for species A and B, respectively). In the case of fermions, the maximal number of particles on the site is $M = 1$.

It is assumed that particles do not have internal degrees of freedom. One species on a single lattice site could be now in $M+1$ different states — there are $0, 1, \ldots, M-1$ or M particles on the site. The Hilbert space of a single site is thus $M + 1$ dimensional space $\mathcal{H}$ ($\mathcal{H}_A$ and $\mathcal{H}_B$ for species A and B, respectively). The eigenvectors of the particle number operator form an orthonormal basis of space $\mathcal{H}$ and all of the following operators are expressed in this basis.

For the construction of the Bose-Hubbards Hamiltonians (4.23), (4.60) and (4.61) it is necessary to construct annihilation operators a, b, creation operators $a^\dagger$, $b^\dagger$, and particle number operator n^A, n^B on the lattice site. The matrix forms of these operators for species A are

$$A = \begin{pmatrix} 0 & \sqrt{1} & 0 & \ldots & 0 \\ 0 & 0 & \sqrt{2} & \ldots & 0 \\ \vdots & \vdots & \vdots & \vdots & \vdots \\ 0 & 0 & 0 & \ldots & \sqrt{M_A} \\ 0 & 0 & 0 & \ldots & 0 \end{pmatrix} \tag{5.3}$$

$$A^\dagger = \begin{pmatrix} 0 & 0 & \ldots & 0 & 0 \\ \sqrt{1} & 0 & \ldots & 0 & 0 \\ 0 & \sqrt{2} & \ldots & 0 & 0 \\ \vdots & \vdots & \vdots & \vdots & \vdots \\ 0 & 0 & \ldots & \sqrt{M_A} & 0 \end{pmatrix} \tag{5.4}$$

$$N_A = A^\dagger A = \begin{pmatrix} 0 & 0 & 0 & \ldots & 0 \\ 0 & 1 & 0 & \ldots & 0 \\ 0 & 0 & 2 & \ldots & 0 \\ \vdots & \vdots & \vdots & \vdots & \vdots \\ 0 & 0 & 0 & \ldots & M_A \end{pmatrix} \tag{5.5}$$

Operators for species B — B,$B^\dagger$, and N_B — are created analogously.

Let us analyze the Bose-Bose Hubbard model (4.60) to understand how the matrix form of the one-site Hamiltonian is constructed. The Hilbert space of the system of both species on a single lattice site is $\mathcal{H}_A \otimes \mathcal{H}_B$. The matrix Hamiltonian of the site is thus:

$$H_S = \frac{1}{2}U_{AA}N_A(N_A - I_A) \otimes I_B + I_A \otimes \frac{1}{2}U_{BB}N_B(N_B - I_B) + U_{AB}N_A \otimes N_B \tag{5.6}$$

where I_A and I_B are unit matrices of dimension $M_A + 1$ and $M_B + 1$, respectively, and $\otimes$ is the *Kronecker product.*

The Hamiltonian H_S and matrix operators A,B,$A^\dagger$,$B^\dagger$,N_A and N_B are used as a basic building blocks of the program.

Weight limit

The are two ways how to select the most important states of the density matrix (5.2). The first one is to select a fixed number of states t_{max} every time. That means the number of states that are stored in every block is also t_{max}. The second way is to store such a number of states t_{lim} that the sum w of the truncated-states weights is lower than some truncation limit w_{lim}:

$$w = 1 - \sum_{i=1}^{t_{lim}} w_i < w_{lim} \tag{5.7}$$

where w_i are the density-matrix weights sorted from the highest to the lowest.

Both methods have advantages and disadvantages. The current implementation of the DMRG algorithm combines both strategies. The t_{lim} most important states are selected. Afterwards, if the number of these states is greater than t_{max}, only the t_{max} states with highest weights are stored. This method ensures:

1. The number of states stored in blocks is small as there are usually only a few states with significant weights. Consequently, it makes the algorithm run much faster.
2. The number of states stored in blocks is fixed. The algorithm will not get stuck due to matrices being too large.

Sweeps

The number of sweeps can be either constant or convergence dependent. In the latter case, after every sweep the energy of the system is compared to the energy of the previous sweep. The sweeping continues until the difference in energies ΔE is lower than a convergence limit s_{lim}.

The sweeping is also performed after every step of the warmup procedure, as it helps to obtain an accurate wavefunction [40].

Phase diagram

One of the differences between the insulator phase and the superfluid phase is the existence of an energy gap in adding or removing a particle. Adding or removing a particle in the insulator phase causes the energy of the system to rise or drop significantly. On the other hand, if the system is in the superfluid phase, the energy difference is negligible.

Therefore one of the ways to determine whether the species is in the insulator phase or in the superfluid phase, is to calculate a phase diagram (4.1).

At the beginning, the ground state energy E_0 for a system with N particles of particular species is calculated. The chemical potential

$$\mu = \left(\frac{\partial U}{\partial N} \right) \tag{5.8}$$

is in fact an increase in energy caused by adding or removing one particle. The ground state energies E_H and E_P for systems with $N - 1$ and $N + 1$ particles are calculated as well. The upper border μ_P and the lower border μ_H is then obtained as:

$$\mu_P = E_P - E_0 \tag{5.9}$$
$$\mu_H = E_0 - E_H \tag{5.10}$$

The chemical potentials μ_P and μ_H differ for a system in the insulator phase. μ_P and μ_H are equal for a system in the superfluid phase.

Using this algorithm it is possible to obtain the phase diagram and to find the critical values of parameters of the transition from the insulating to the superfluid phase.

5.4 Implementation testing

To test the DMRG implementation for two-species bosonic systems, the model systems from Ref. [40] were recalculated. Particle density graphs in Figure 5.2 and Figure 5.3 agree with graphs given in the the reference. This should be re-assuring that the implementation is correct.

Figure 5.2: Particle density for two bosonic species A and B for two values of U: Model parameters: $J_A = J_B = 1$, $U_A = U_B = U$, $U_{AB} = 1.05 \times U$. Particle densities: $\rho_A = \rho_B = 0.5$. Calculation parameters: number of sites $N = 50$, number of sweeps $s = 10$ (with additional sweeps during every step of warmup procedure, as mentioned in the reference), maximal number of particles at a site $M_A = 3$, $M_B = 3$, truncation weight limit $w_{lim} = 5 \times 10^{-5}$, truncation states limit $t_{max} = 128$. The results are identical to Ref. [40]

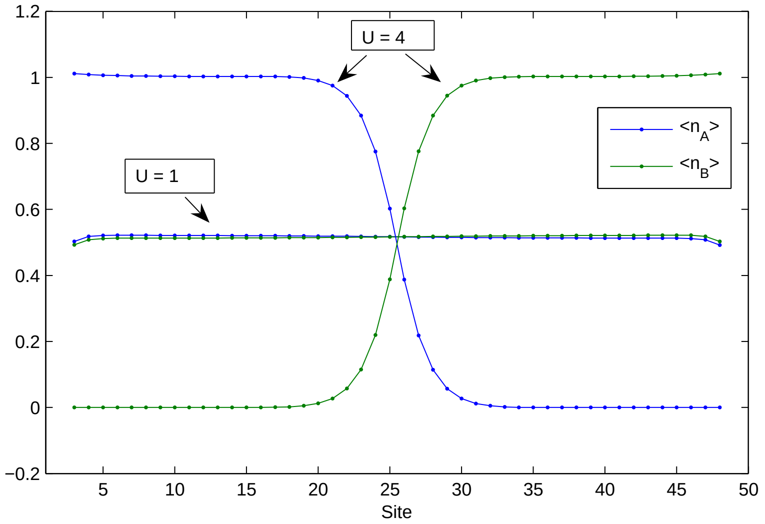

Figure 5.3: Particle density for two bosonic species A and B for two values of U: Model parameters: $J_A = J_B = 1$, $U_A = U_B = U$, $U_{AB} = 1.05 \times U$. Particle densities: $\rho_A = 1$, $\rho_B = 0.5$. Calculation parameters: number of sites $N = 50$, number of sweeps $s = 10$ (with additional sweeps during every step of warmup procedure, as mentioned in the reference), maximal number of particles at a site $M_A = 3$, $M_B = 3$, truncation weight limit $w_{lim} = 5 \times 10^{-5}$, truncation states limit $t_{max} = 128$.The results are identical to Ref. [40]

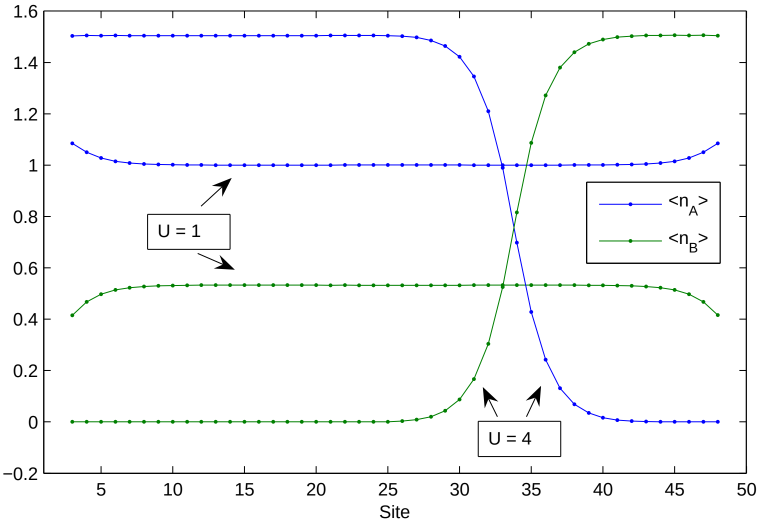

Chapter 6

Results

This section focuses on the analysis of real mixtures in 1D optical lattices, particularly on the ^{87}Rb^{133}Cs and ^{6}Li^{133}Cs mixtures. The former is a boson-boson mixture, whereas the latter is a boson-fermion mixture. In the first part, the role of the optical potential for different detuning schemes is investigated and the possible model parameters are determined. The systems are analysed for a particular parameter selections in the second part.

6.1 Optical potential

The strength of the optical potential (2.20) depends on the laser wavelength, intensity and on the properties of trapped atoms. It differs for different species. Figures 6.2 and 6.1 show the optical potential strength dependency on the wavelength for RbCs and LiCs mixtures, respectively. The wavelengths of lithium resonance lines D_1 and D_2 are very close, therefore it can be considered as one line only.

It is possible to identify following detuning regions:

- **A,C**: The laser is blue-detuned for both species, thus both atoms are trapped at the positions, where the laser intensity is minimal.
- **B,D,F**: The laser is red-detuned for one species and blue-detuned for the other. The lattices for both species are thus shifted in space by $\lambda/4$. The interaction between species is small if the lattices are deep. It is thus possible to describe it as the two independent one-species Bose-Hubbard models. More accurate description would include an interaction between neighbouring sites of the two lattices, which is important in the case of shallow lattices. Note that in the RbCs and LiCs cases, the laser is always blue detuned for caesium atoms. The caesium atoms are thus trapped at the places of maximal laser intensity.
- **E,G**: The laser is red-detuned for both species, thus they are trapped at the positions of maximal laser intensity.

The favoured detuning strategy is a far detuned laser for the following reasons:

- The saturation is negligible.
- The scattering rate (2.21) is low.

Figure 6.1: Optical potential for RbCs for a laser intensity $I = 1 \times 10^7$ W m^{-2}. Blue line is the rubidium optical potential and the green line is the caesium optical potential.

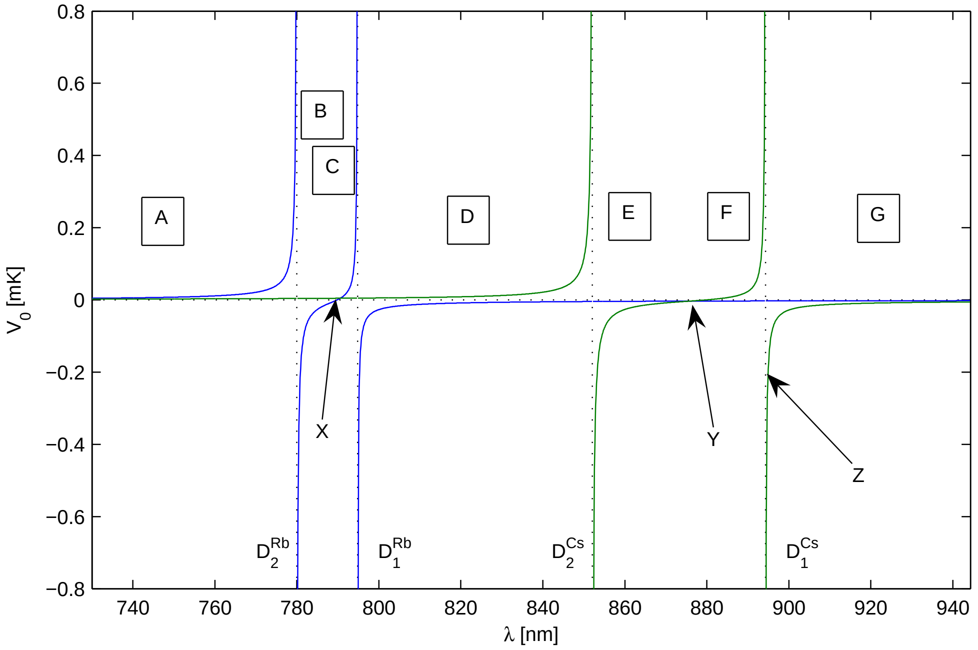

Figure 6.2: Optical potential for LiCs for a laser intensity $I = 1 \times 10^7$ W m^{-2}. Blue line is the lithium optical potential and the green line is the caesium optical potential.

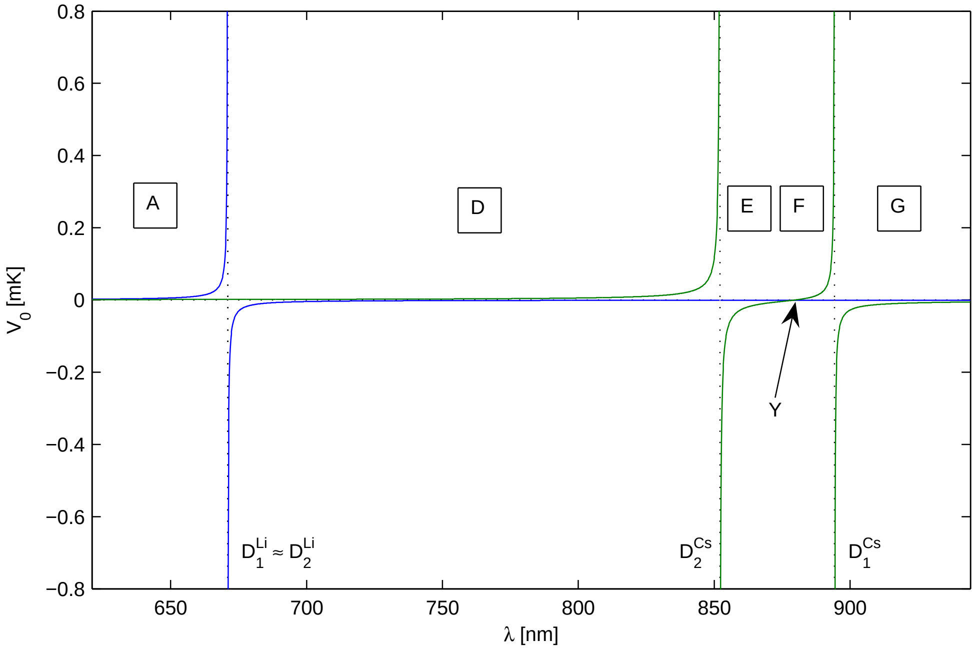

Using a formula (2.23) it is possible to calculate the forbidden detunings due to saturation. The forbidden regions are showed in Figure 6.3 for laser light intensity $I = 1 \times 10^7$ W m^{-2} and population ratio $k = 10^{-6}$.

Figure 6.3: The detail of optical potential in Figure 6.2 showing forbidden regions due to high saturation for laser intensity $I = 1 \times 10^7$ W m^{-2}. For the laser wavelength in grey regions, proportion of atoms in excited state and in the ground state is higher than $k = 10^{-6}$. Such detunings are thus unfavourable in experiments.

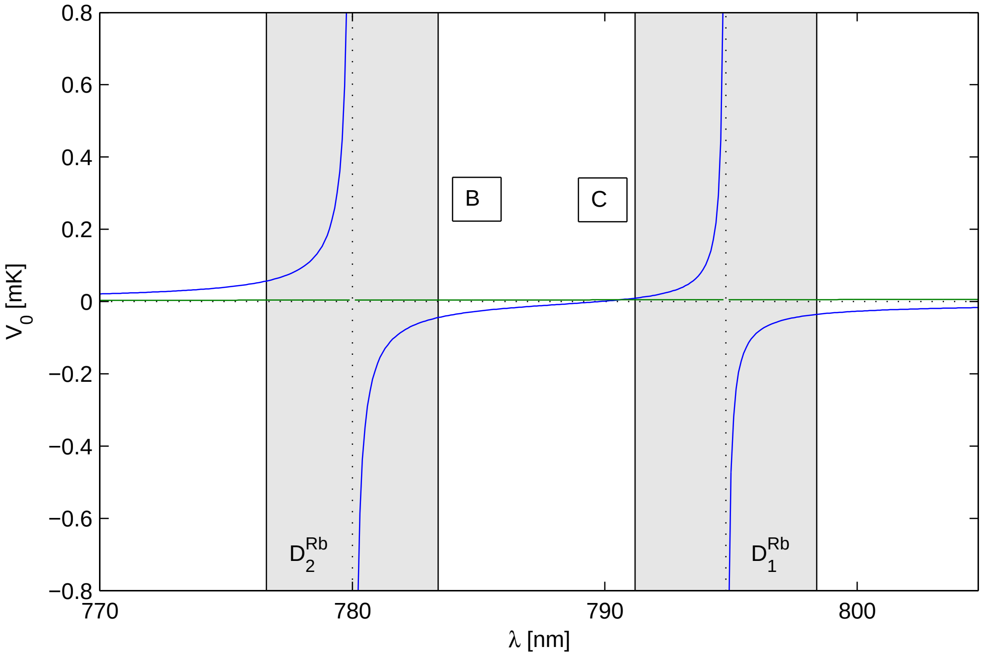

Current experiments are typically performed with a far detuned laser wavelength in the G region, for example with a wavelength $\lambda = 1064$ nm [41]. However, Ref. [18] suggests to use also a near detuned laser in experiments. There exist two particularly interesting schemes:

- To tune the laser to a wavelength such that the strength of the optical potential vanishes for one species. Such a species becomes a background atomic gas, whereas the second species is confined to the lattice. The corresponding wavelengths are denoted as X and Y in the figures above.
- To tune the laser close to resonance of one species. The optical potential for that species becomes very strong, whereas the second one is trapped with only small force. An example of such a wavelength is denoted as Z in the above figures.

Detailed analysis of possible species pair for these schemes is given in [18]. Such configurations can introduce new effect to lattice experiments, for example a possibility of existence of phonons in the lattice. However, the practical feasibility of these schemes has to be investigated yet.

Trapping both species at the same space position is more interesting. In the following, the description is thus restricted to the regions A,C,E, and G.

6.2 Model parameters

The parameters of the two-species Bose-Hubbard model, (4.28), (4.29), and (4.62), depend on the laser wavelength, the laser intensity, and the species properties. If the pair of species is given, it is only possible to modify the parameters by changing the laser wavelength and intensity. The possible parameter ranges are investigated in this section.

First of all, note that the optical potential (2.20) depends linearly on the light intensity. Using this fact in formulae (4.28) and (4.62) it turns out that the ratio $U_{AA} : U_{BB} : U_{AB}$ is independent of the laser intensity. Thus for a fixed wavelength it is possible to change the ratio of J_A and J_B to $U_{AA} : U_{BB} : U_{AB}$ only. If the intensity is high, hopping terms J_A and J_B become small.

The confinement in transverse direction must be strong enough to create a 1D system. The transverse trapping potential in Ref. [19] was $V_0^{\perp} = 30E_R$. Similar values are to be used here. To confine both species for every pair, an appropriate wavelength has to be chosen.

To determine interaction parameters for a pair of particular species, it is necessary to known the corresponding scattering length a. The scattering length depends on the hyperfine states of atoms. In actual experiments, the atoms are usually prepared in a particular hyperfine state before the experiment. The description in the following sections is thus restricted to particular cases only.

^{87}Rb^{133}Cs

Let us suppose that rubidium atoms are in the $|F = 3/2, m_F = 3/2\rangle$ hyperfine state and caesium atoms are in the $|F = 7/2, m_F = 7/2\rangle$ state. The spin projections of their valence electrons are identical. The intraspecies, as well as the interspecies interactions are thus described by the triplet scattering length. The value of $a = 700a_0$ from Table 4.1 is used in the following calculations. The dependency on the laser wavelength for particular parameters is in Figure (6.4). Note that interaction terms U_{AA}, U_{BB}, and U_{AB} do not change very much with the wavelength.

^{6}Li^{133}Cs

Similarly to the previous case, let us suppose both species are in their doubly polarized states; that is the lithium atoms are in the $|F = 3/2, m_F = 3/2\rangle$ state and caesium atoms are in the $|F = 7/2, m_F = 7/2\rangle$ state. However, the triplet scattering length for ^{6}Li^{133}Cs was not available at the time of writing. The only available data, the singlet scattering length for ^{7}Li^{133}Cs was used instead ($a = 50a_0$). This substitution is not very appropriate, but it is a best that can be done at this time. When the new data are available, it is possible to recalculate the model. The dependency on the laser wavelength is in the Figure (6.5). The interaction terms U_{AA}, U_{BB}, and U_{AB} does not depend very much on the detuning in this case as well.

Figure 6.4: Dependency of the Bose-Hubbard model parameters on the laser wavelength for species A = ^{87}Rb and B = ^{133}Cs. The laser wavelength in transverse direction is $\lambda^{\perp} = 1064$ nm and the laser intensity is $I^{\perp} = 2 \times 10^{7}$ W m^{-2}. The corresponding optical potentials are $V_A^{\perp} = 27E_{RA}$, $V_B^{\perp} = 72E_{RB}$, where E_{RA} and E_{RB} are the recoil energies for species A and B, respectively. Laser intensity in the axial direction is $I^{\parallel} = 2 \times 10^{6}$ W m^{-2}. The wavelength is restricted to the A,C,E,G regions mentioned in the previous sections and detuned at least 4 nm from the resonance to take account of the saturation.

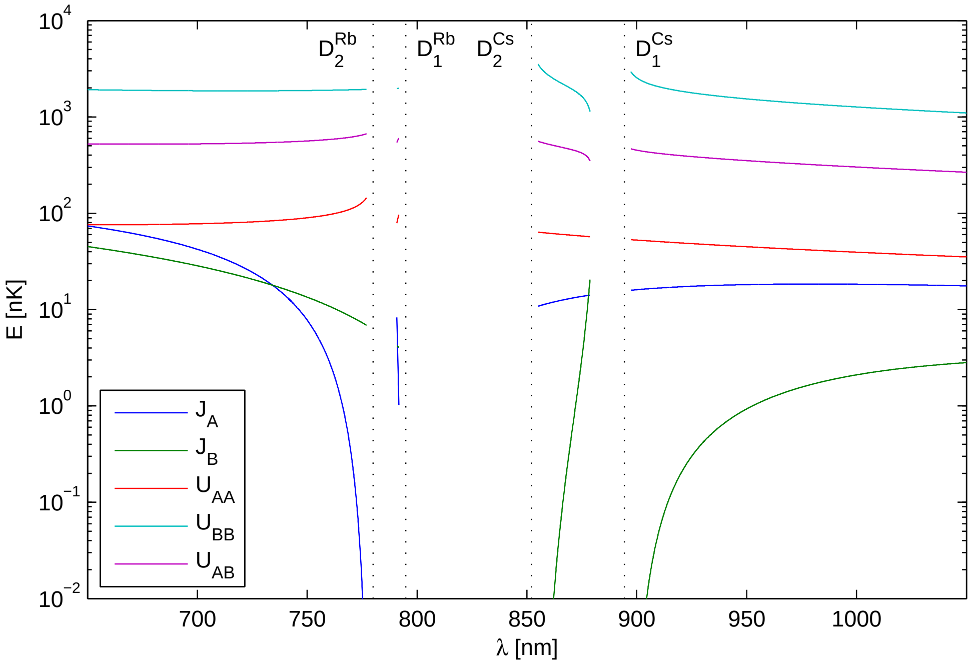

Figure 6.5: Dependency of the Bose-Hubbard model parameters on the laser wavelength for species A = ^{6}Li and B = ^{133}Cs. The laser wavelength in transverse direction is $\lambda^\perp = 665$ nm and the laser intensity is $I^\perp = 6 \times 10^7$ W m^{-2}. The corresponding optical potentials are $V_A^\perp = 34E_{RA}$, $V_B^\perp = 52E_{RB}$, where E_{RA} and E_{RB} are the recoil energies for species A and B, respectively. Laser intensity in the axial direction is $I^\parallel = 6 \times 10^6$ W m^{-2}. The wavelength is restricted to the A,E,G regions mentioned in the previous sections and detuned at least 4 nm from the resonance to take account of the saturation.

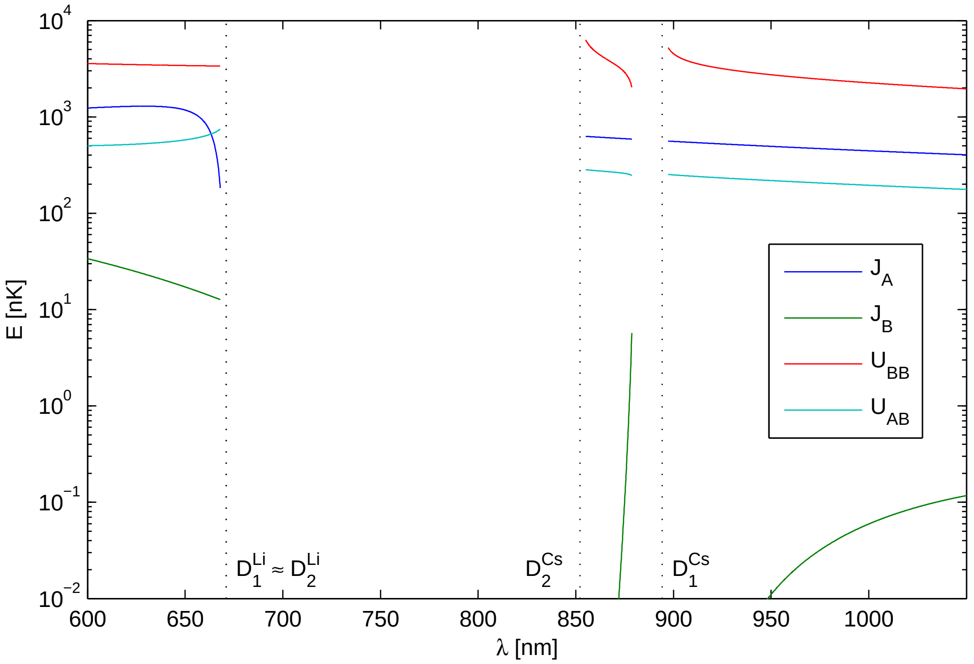

6.3 RbCs mixture

The ^{87}Rb^{133}Cs mixture is modelled on a lattice of $N = 50$ sites. The external trapping potential of the two-species Bose-Hubbard model is not considered ($V_i^A = V_i^B = 0$). The laser wavelength is $\lambda = 1064$ nm in all three spatial directions. The transverse optical potential is $I^{\perp} = 2 \times 10^7$ W m^{-2}. The dependence of the system ground state on the laser intensity in the axial direction is studied for various total particle densities ρ_A and ρ_B (the number of particles on the lattice is $N\rho_A$ and $N\rho_B$).

The particle density distributions for $\rho_A = 0.5$ and $\rho_B = 0.5$ are in the Figure 6.6, and the corresponding phase diagram is in the Figure 6.7.

For low laser intensities, both species are superfluid and delocalized. Rubidium atoms are slightly compressed. As the intensity grows, the atoms become more localized. The phase transition between the insulating and the superfluid phase occurs approximately at the laser intensity of $I^{\parallel} = 2 \sim 3 \times 10^6$ W m^{-2}. The most distinct feature is the phase separation — the particles of the same species tend to stick together. There is almost no overlap between rubidium and caesium atoms.

The results for $\rho_A = 1.0$ and $\rho_B = 0.5$ are in the Figures 6.8 and 6.9. In this case the particle density distribution does not change very much with the laser intensity. However, as can be seen from the phase diagram, there is a phase transition from the superfluid to the insulator phase that occurs at $I^{\parallel} = 3 \sim 4 \times 10^6$ W m^{-2}. The mixture is phase separated as well.

In case of densities $\rho_A = 1.0$ and $\rho_B = 1.0$, as can be seen in the Figure 6.10, the phases are not separated any more. Both species tend to occupy whole lattice. Rubidium is superfluid for the low laser intensities and insulating for the high intensities.

6.4 LiCs mixture

The ^{6}Li^{133}Cs mixture is modelled on a lattice of $N = 50$ sites. The external trapping potential of the two-species Bose-Hubbard model is not considered ($V_i^A = V_i^B = 0$). The laser wavelength is $\lambda = 665$ nm in all three spatial directions. The transverse optical potential is $I^{\perp} = 6 \times 10^7$ W m^{-2}.

The dependence of the system ground state on the laser intensity in the axial direction is studied for total particle densities $\rho_A = 0.5$ and $\rho_B = 0.5$ are in the Figure 6.11.

The figure significantly differs from the RbCs case. The particles form an alternating periodic structure. For low intensities, both species are delocalized on the whole lattice. As the intensity grows, both species are still delocalized, but start to alternate in the lattice. This corresponds to the supersolid phase [34]. The caesium atoms become localized for a moderately deep lattice at the laser intensity about $I^{\parallel} = 6 \times 10^6$ W m^{-2}. If the laser intensity is high enough, both species become localized at alternating sites. This correspond to the charge density wave phase [34].

Figure 6.6: Particle density for a system of two bosonic species A = ^{87}Rb (blue) and B = ^{133}Cs (green) on a lattice with 50 sites for different laser intensities. Total particle densities are $\rho_A = 0.5$ and $\rho_B = 0.5$. Lattice parameters: $\lambda^{\perp} = \lambda^{\parallel} = 1064$ nm, $I^{\perp} = 2 \times 10^7$ W m^{-2} (the corresponding transverse optical potentials are $V_A^{\perp} = 27 E_{RA}$ and $V_B^{\perp} = 71 E_{RB}$). Calculation parameters: maximum number of particles on a site $M_A = M_B = 4$, truncation weight limit $w_{lim} = 10^{-5}$, truncation states limit $t_{max} = 128$, sweeping convergence limit $s_{lim} = 10^{-10}$. The energy is rescaled so that $U_{AB} = 1$. The ratio of interaction parameters does not depend on the laser intensity: $U_A = 0.1324$, $U_B = 4.1045$, $U_{AB} = 1$.

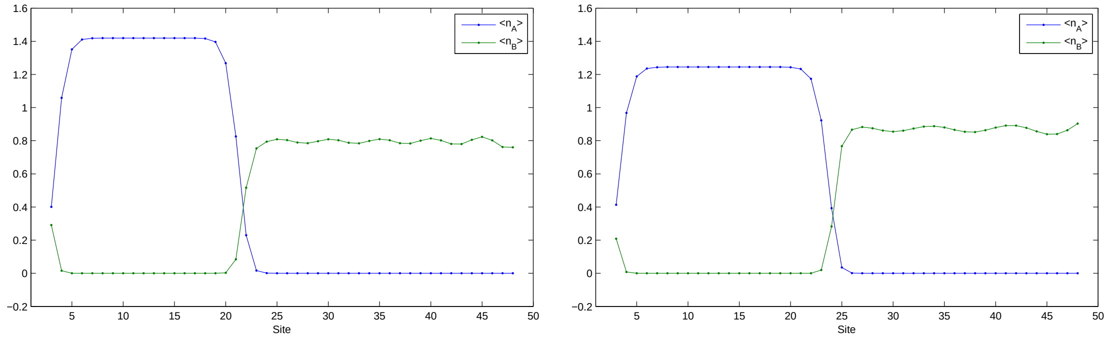

$I^{\parallel} = 5 \times 10^5$ W m^{-2}
$J_A = 0.1733, J_B = 0.0835$

$I^{\parallel} = 8 \times 10^5$ W m^{-2}
$J_A = 0.1419, J_B = 0.0518$

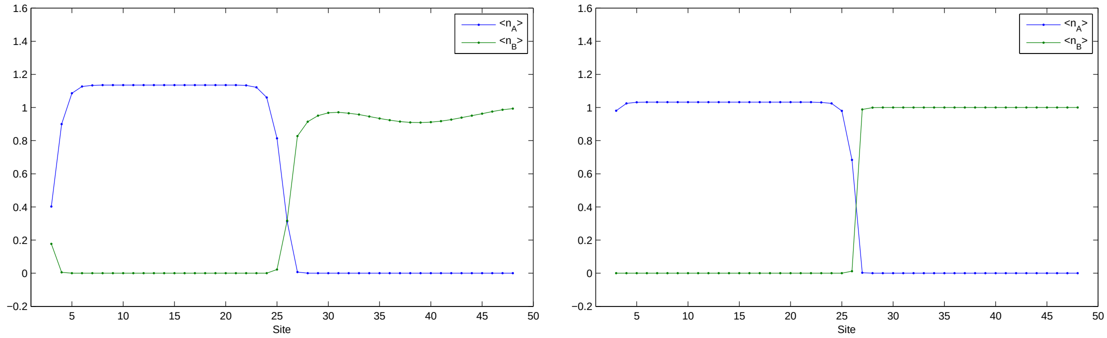

$I^{\parallel} = 1 \times 10^6$ W m^{-2}
$J_A = 0.1242, J_B = 0.0388$

$I^{\parallel} = 2 \times 10^6$ W m^{-2}
$J_A = 0.0672, J_B = 0.0114$

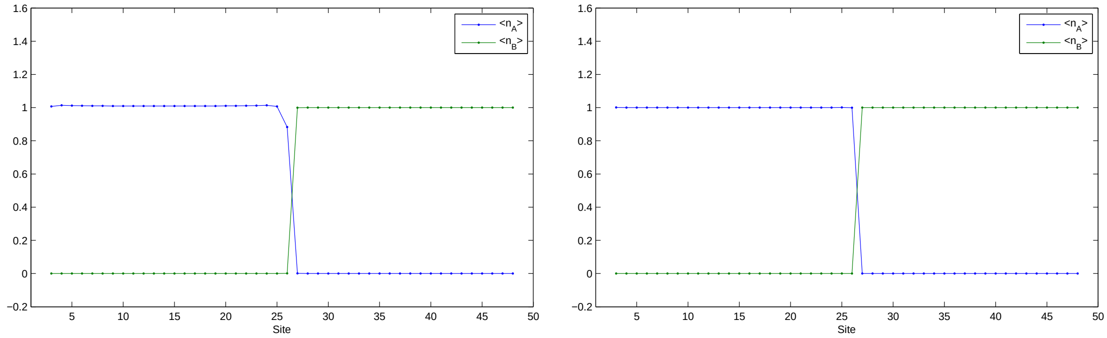

$I^{\parallel} = 3 \times 10^6$ W m^{-2}
$J_A = 0.0394, J_B = 0.0042$

$I^{\parallel} = 6 \times 10^6$ W m^{-2}
$J_A = 0.0105, J_B = 0.0004$

Figure 6.7: Phase diagram corresponding to the Fig. 6.6. The part between the lines is the insulating phase. The phase transition occurs where the two lines meet. It can be deduced that the phase transition occurs approximately at $J_A \approx 0.05$. The lines do not meet accurately due to finite lattice size.

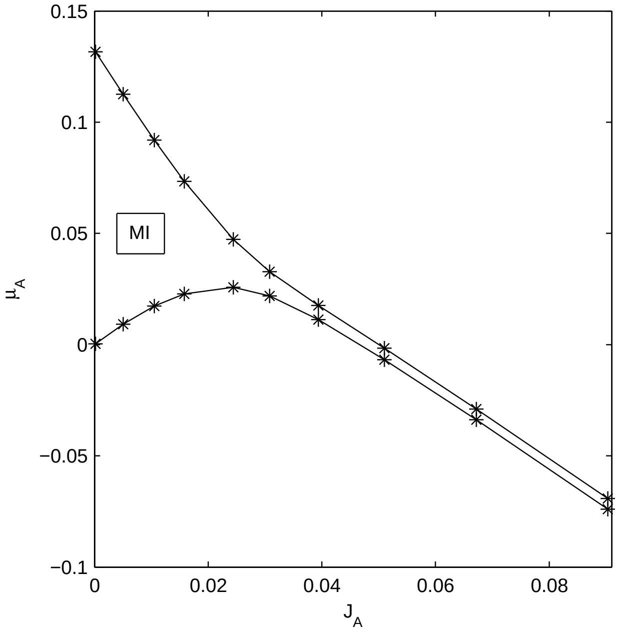

Figure 6.8: Particle density for a system of two bosonic species A = ^{87}Rb (blue) and B = ^{133}Cs (green) on a lattice with 50 sites for different laser intensities. Total particle densities are $\rho_A = 1.0$ and $\rho_B = 0.5$. Lattice parameters: $\lambda^{\perp} = \lambda^{\parallel} = 1064$ nm, $I^{\perp} = 2 \times 10^7$ W m^{-2} (the corresponding transverse optical potentials are $V_A^{\perp} = 27E_{RA}$ and $V_B^{\perp} = 71E_{RB}$). Calculation parameters: maximum number of particles on a site $M_A = M_B = 4$, truncation weight limit $w_{lim} = 10^{-5}$, truncation states limit $t_{max} = 128$, sweeping convergence limit $s_{lim} = 10^{-10}$. The energy is rescaled so that $U_{AB} = 1$. The ratio of interaction parameters does not depend on the laser intensity: $U_A = 0.1324$, $U_B = 4.1045$, $U_{AB} = 1$.

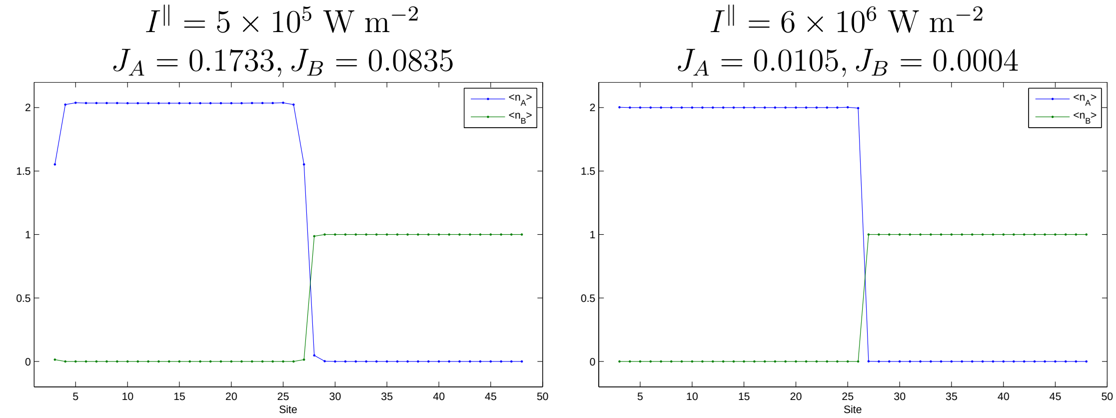

$I^{\parallel} = 5 \times 10^5$ W m^{-2}
$J_A = 0.1733, J_B = 0.0835$

$I^{\parallel} = 6 \times 10^6$ W m^{-2}
$J_A = 0.0105, J_B = 0.0004$

Figure 6.9: Phase diagram corresponding to the Fig. 6.8. The part between the lines is the insulating phase. The phase transition occurs where the two lines meet. It can be deduced that the phase transition occurs approximately at $J_A \approx 0.03$. The lines do not meet accurately due to finite lattice size.

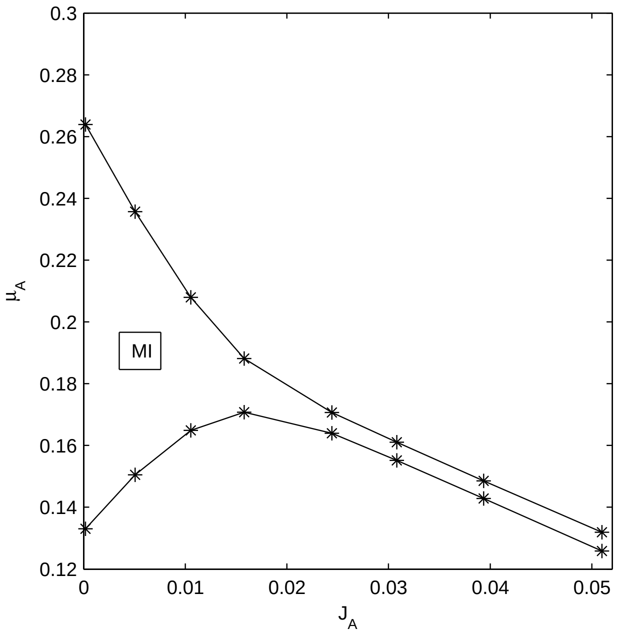

Figure 6.10: Particle density for a system of two bosonic species A = ^{87}Rb (blue) and B = ^{133}Cs (green) on a lattice with 50 sites for different laser intensities. Total particle densities are $\rho_A = 1.0$ and $\rho_B = 1.0$. Lattice parameters: $\lambda^{\perp} = \lambda^{\parallel} = 1064$ nm, $I^{\perp} = 2 \times 10^7$ W m^{-2} (the corresponding transverse optical potentials are $V_A^{\perp} = 27E_{RA}$ and $V_B^{\perp} = 71E_{RB}$). Calculation parameters: maximum number of particles on a site $M_A = M_B = 4$, truncation weight limit $w_{lim} = 10^{-5}$, truncation states limit $t_{max} = 128$, sweeping convergence limit $s_{lim} = 10^{-10}$. The energy is rescaled so that $U_{AB} = 1$. The ratio of interaction parameters does not depend on the laser intensity: $U_A = 0.1324$, $U_B = 4.1045$, $U_{AB} = 1$.

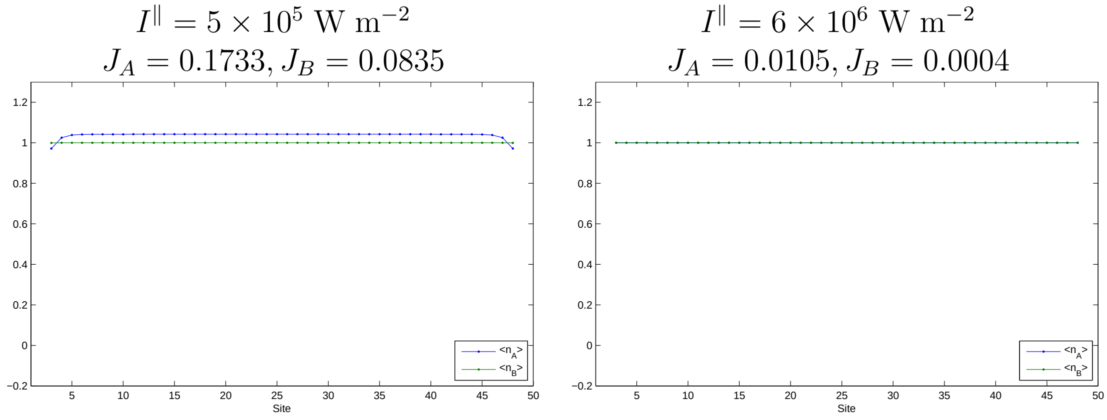

$I^{\parallel} = 5 \times 10^5$ W m^{-2}
$J_A = 0.1733, J_B = 0.0835$

$I^{\parallel} = 6 \times 10^6$ W m^{-2}
$J_A = 0.0105, J_B = 0.0004$

Figure 6.11: Particle density for a mixture of fermionic species A = ^{6}Li (blue) and bosonic species B = ^{133}Cs (green) on a lattice with 50 sites for different laser intensities. Total particle densities are $\rho_A = 0.5$ and $\rho_B = 0.5$. Lattice parameters: $\lambda^{\perp} = \lambda^{\parallel} = 665$ nm, $I^{\perp} = 6 \times 10^{7}$ W m^{-2} (the corresponding transverse optical potentials are $V_A^{\perp} = 34E_{RA}$ and $V_B^{\perp} = 52E_{RB}$). Calculation parameters: maximum number of particles on a site $M_A = 1$, $M_B = 4$, truncation weight limit $w_{lim} = 10^{-5}$, truncation states limit $t_{max} = 128$, sweeping convergence limit $s_{lim} = 10^{-10}$. The energy is rescaled so that $U_{AB} = 1$. The ratio of interaction parameters does not depend on the laser intensity: $U_B = 4.9204$, $U_{AB} = 1$.

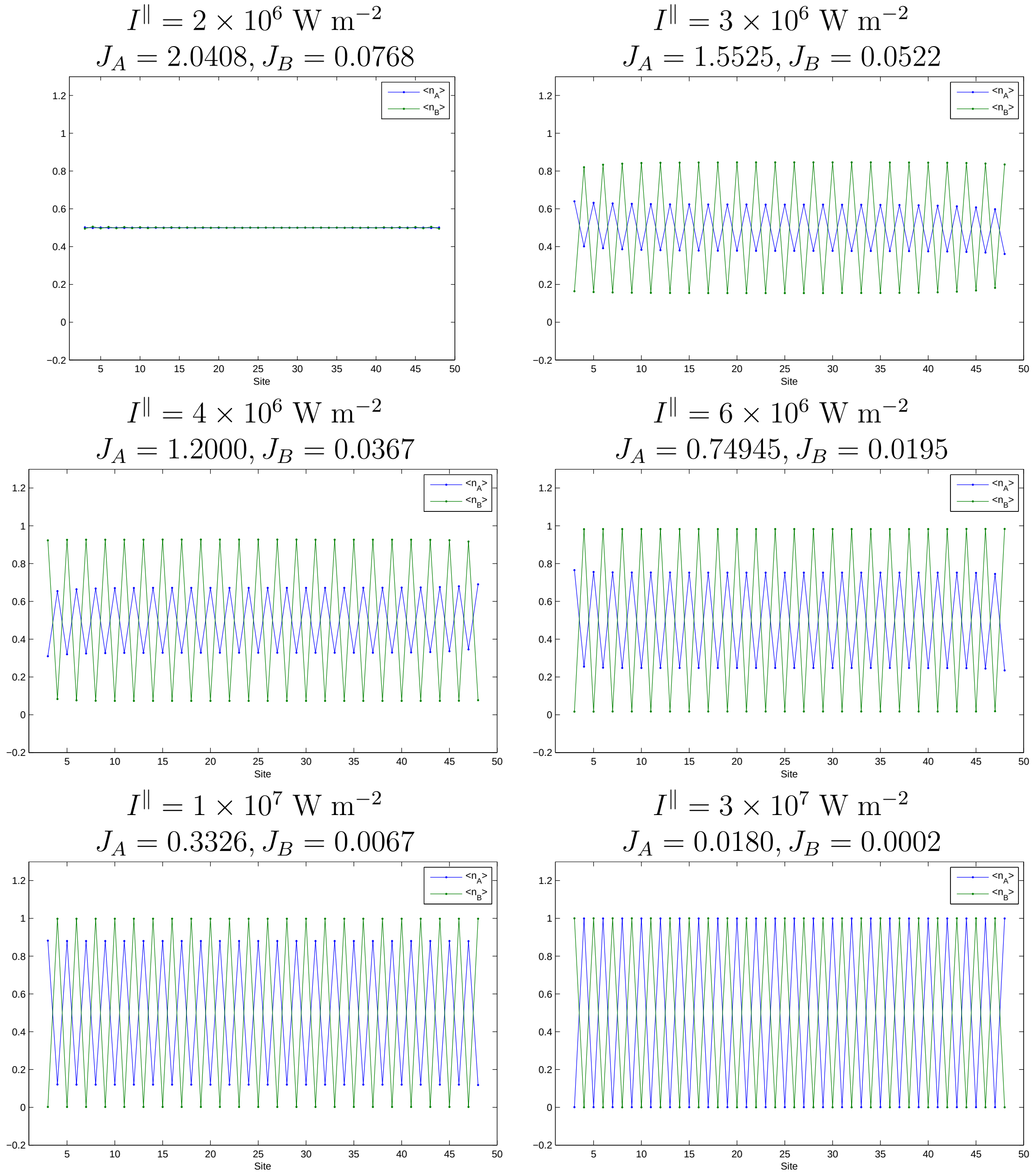

$I^{\parallel} = 2 \times 10^{6}$ W m^{-2}
$J_A = 2.0408$, $J_B = 0.0768$

$I^{\parallel} = 3 \times 10^{6}$ W m^{-2}
$J_A = 1.5525$, $J_B = 0.0522$

$I^{\parallel} = 4 \times 10^{6}$ W m^{-2}
$J_A = 1.2000$, $J_B = 0.0367$

$I^{\parallel} = 6 \times 10^{6}$ W m^{-2}
$J_A = 0.74945$, $J_B = 0.0195$

$I^{\parallel} = 1 \times 10^{7}$ W m^{-2}
$J_A = 0.3326$, $J_B = 0.0067$

$I^{\parallel} = 3 \times 10^{7}$ W m^{-2}
$J_A = 0.0180$, $J_B = 0.0002$

Conclusions

The properties of binary mixtures in one-dimensional optical lattices were investigated on various levels. The approximate formulae for the parameters of the binary Bose-Hubbard model based on real experimental parameters were derived. Selected mixtures were analysed numerically, using the DMRG algorithm.

The dominating effect in the RbCs and LiCs mixtures is the heavy weight and large scattering length of caesium atoms. The tunnelling in the lattice is low and the intraspecies repulsion is high, thus there is usually up to a one caesium atom on a lattice site.

It was found that ^{87}Rb^{133}Cs mixtures are phase separated for low density parameters. The same species tend to stick together, and the mixture phase varies from superfluid to insulator as the laser intensity grows.

On the other hand, ^{6}Li^{133}Cs mixtures tend to form alternating-species structures. For low laser intensities the mixture is in the supersolid phase; for high intensities it is in the charge density wave phase. However, the LiCs calculation used a non-appropriate scattering length, because the accurate value was not available at the time of writing. The LiCs calculation thus cannot be considered quantitatively correct. It serves primarily as an example. A new calculation will have to be performed when the scattering data will become available.

Currently, there are no known experimental results concerning binary mixtures in 1D optical lattices. If such experiments are performed, it will be interesting to compare the results.

Possible continuations of this work include:

1. To perform calculations using a model with an external trapping potential. In case of the harmonic trapping potential, the model lattice should have at least 100 sites to observe trapping effect for real parameter ranges. Another interesting model introduces random disorder potential which gives rise to a special phase — Bose-Glass phase.

2. Analysis of the 2D and 3D cases.

Bibliography

[1] D. Jaksch, C. Bruder, J. I. Cirac, C. W. Gardiner, and P. Zoller, “Cold Bosonic Atoms in Optical Lattices,” *Physical Review Letters* **81** (1998) 3108–3111.

[2] T. D. Kühner and H. Monien, “Phases of the one-dimensional Bose-Hubbard model,” *Physical Review B* **58** (1999) 14741.

[3] M. Greiner, O. Mandel, T. Esslinger, T. W. Hänsch, and I. Bloch, “Quantum phase transition from a superfluid to a Mott insulator in a gas of ultracold atoms,” *Nature* **419** (2002) 39–44.

[4] K. Günter, T. Stöferle, H. Moritz, M. Köhl, and E. T., “Bose-Fermi Mixtures in a Three-Dimensional Optical Lattice,” *Physical Review Letters* **96** (2006) 180402.

[5] S. Ospelkaus, C. Ospelkaus, O. Wille, M. Succo, P. Ernst, K. Sengstock, and K. Bongs, “Localization of Bosonic Atoms by Fermionic Impurities in a Three-Dimensional Optical Lattice,” *Physical Review Letters* **96** (2006) 180403.

[6] L. Pollet, C. Kollath, U. Schollwöck, and M. Troyer, “Mixture of bosonic and spin-polarized fermionic atoms in an optical lattice,” *Physical Review A* **77** (2008) 023608.

[7] U. Schollwöck, “The density-matrix renormalization group,” *Reviews of Modern Physics* **77** (2005) 259.

[8] MathWorks, “MATLAB.” `http://www.mathworks.com/`.

[9] R. Shankar, *Principles of Quantum Mechanics, Second edition.* Plenum Press, New York, 1994.

[10] C. Pethick and H. Smith, *Bose-Einstein Condensation in Dilute Gases.* Cambridge University Press, Cambridge, 2002.

[11] “Wikipedia, the free encyclopedia.” `http://www.wikipedia.org/`.

[12] C. J. Foot, *Atomic Physics.* Oxford University Press, Oxford, 2005.

[13] M. E. Gehm, “Properties of ^{6}Li.” `http://www.phy.duke.edu/research/photon/qoptics/techdocs/`, 2003.

[14] D. A. Steck, "Sodium D Line Data." Los Alamos National Laboratory Report LA-UR-03-8639, `http://www.steck.us/alkalidata/`, 2003.

[15] D. A. Steck, "Rubidium 87 D Line Data." Los Alamos National Laboratory Report LA-UR-03-8638, `http://www.steck.us/alkalidata/`, 2003.

[16] D. A. Steck, "Cesium D Line Data." Los Alamos National Laboratory Report LA-UR-03-7943, `http://www.steck.us/alkalidata/`, 2003.

[17] R. Grimm, M. Weidemüller, and Y. B. Ovchinnikov, "Optical dipole traps for neutral atoms," *Advances in Atomic, Molecular and Optical Physics* **42** (2000) 95–170.

[18] L. J. LeBlanc and J. H. Thywissen, "Species-specific optical lattices," *Physical Review A* **75** (2007) 053612.

[19] T. Stöferle, H. Moritz, C. Schori, M. Köhl, and T. Esslinger, "Transition from a strongly interacting 1D superfluid to a Mott insulator," *Physical Review Letters* **92** (2004) 130403.

[20] B. Paredes, A. Widera, V. Murg, O. Mandel, S. Fölling, I. Cirac, G. V. Shlyapnikov, T. W. Hänsch, and I. Bloch, "Tonks-Girardeau gas of ultracold atoms in an optical lattice," *Nature* **429** (2004) 277–281.

[21] T. Jones, "Mathieu's Equations and the Ideal rf-Paul Trap." `http://www.physics.drexel.edu/~tim/open/mat/`.

[22] J. E. Sträng, "On the characteristic exponents of Floquet solutions to the Mathiue equation," *Academic Royale de Belgique, Bulletin de la classe des Sciences* **6** (2005) 269–287.

[23] W. Kohn, "Analytic Properties of Bloch Waves and Wannier Functions," *Physical Review* **115** (1959) 809.

[24] A. M. Rey, *Ultracold bosonic atoms in optical lattices.* PhD thesis, University of Maryland, 2004.

[25] A. Pashov, O. Docenko, M. Tamanis, R. Ferber, H. Knöckel, and T. E., "Coupling of the $X^1\Sigma^+$ and $a^3\Sigma^+$ states of KRb," *Physical Review A* **76** (2007) 022511.

[26] E. Tiesinga, M. Anderlini, and A. E., "Determination of the scattering lenght of the $a^3\Sigma^+$ potential of ^{87}RbCs," *Physical Review A* **75** (2007) 022707.

[27] P. Staanum, A. Pashov, H. Knöckel, and E. Tiemann, "$X^1\Sigma^+$ and $a^3\Sigma^+$ states of LiCs studied by Fourier-transform spectroscopy," *Physical Review A* **75** (2007) 042513.

[28] J. Formánek, *Úvod do kvantové teorie (Introduction to Quantum Theory), Second edition.* Academia, Prague, 2004.

[29] D. Jaksch and P. Zoller, "The cold atom Hubbard toolbox," *Annals of Physics* **315** (2005) 52–79.

[30] A. Albus, F. Illuminati, and E. J., "Mixtures of Bosonic and Fermionic Atoms in Optical Lattices," *Physical Review A* **68** (2003) 023606.

[31] E. Altman, W. Hofstetter, E. Demler, and M. D. Lukin, "Phase diagram of two-component bosons on an optical lattice," *New Journal of Physics* **5** (2003) 113.

[32] I. Bloch, J. Dalibard, and W. Zwerger, "Many-Body Physics with Ultracold Gases," `arXiv:0704.3011v2 [cond-mat.other]`.

[33] A. Mering and M. Fleischhauer, "One-dimensional Bose-Fermi-Hubbard model in the heavy-fermion limit," *Physical Review A* **77** (2008) 023601.

[34] I. Titvinidze, M. Snoek, and W. Hofstetter, "Supersolid Bose-Fermi Mixtures in Optical Lattices," *Physical Review Letters* **100** (2008) 100401.

[35] S. R. White, "Density Matrix Formulation for Quantum Renormalization Groups," *Physical Review Letters* **69** (1992) 2863.

[36] S. R. White, "Density-matrix algorithms for quantum renormalization groups," *Physical Review B* **48** (1993) 10345.

[37] S. Ejima, F. Gebhard, and S. Nishimoto, "Accurate calculation of the Tomonaga-Luttinger parameter K_ρ using the density-matrix renormalization group method," in *Physica B: Condensed MatterVolumes 378-380, Proceedings of the International Conference on Strongly Correlated Electron Systems - SCES 2005*, pp. 304–305. 2006.

[38] M. A. Martín-Delgado, G. Sierra, and R. M. Noack, "The density matrix renormalization group applied to single particle quantum mechanics," *Journal of Physics A* **32** (1999) 6079.

[39] M. Urbanek, "Bose Gases in One-Dimensional Optical Lattices." Unpublished, 2006.

[40] T. Mishra, R. V. Pai, and B. P. Das, "Phase separation in a two-species Bose mixture," *Physical Review A* **76** (2007) 013604.

[41] S. L. Cornish and H.-C. Nägerl. Private communications.

[42] P. Soldán, "Boseho-Einsteinova kondenzace: od atomů k molekulám," *Československý časopis pro fyziku 1/2008* (2008) 4.

[43] P. Sengupta and L. P. Pryadko, "Quantum degenerate Bose-Fermi mixtures on one-dimensional optical lattices," *Physical Review B* **75** (2007) 132507.

[44] L. Guo, Y. Zhang, and S. Chen, "Ground-state competition of two-component bosons in an optical lattice near a Feshbach resonance," *Physical Review A* **75** (2007) 013622.

[45] O. Morsch and M. Oberthaler, “Dynamics of Bose-Einstein condensates in optical lattices,” *Reviews of Modern Physics* **78** (2005) 179.

[46] H. J. Metcalf and P. van der Straten, *Laser Cooling and Trapping.* Springer-Verlag, New York, 1999.